

# Condition numbers in multiview geometry, instability in relative pose estimation, and RANSAC

Hongyi Fan, Joe Kileel, and Benjamin Kimia

**Abstract**—In this paper we introduce a general framework for analyzing the numerical conditioning of minimal problems in multiple view geometry, using tools from computational algebra and Riemannian geometry. Special motivation comes from the fact that relative pose estimation, based on standard 5-point or 7-point Random Sample Consensus (RANSAC) algorithms, can fail even when no outliers are present and there is enough data to support a hypothesis. We argue that these cases arise due to the intrinsic instability of the 5- and 7-point minimal problems. We apply our framework to characterize the instabilities, both in terms of the world scenes that lead to infinite condition number, and directly in terms of ill-conditioned image data. The approach produces computational tests for assessing the condition number before solving the minimal problem. Lastly synthetic and real data experiments suggest that RANSAC serves not only to remove outliers, but also to select for well-conditioned image data, as predicted by our theory.

**Index Terms**—multiview geometry, minimal problems, structure-from-motion, robust estimation, condition numbers, discriminants

## 1 INTRODUCTION

THE past two decades have seen an explosive growth of multiview geometry applications such as the reconstruction of 3D object models for use in video games [1], film [31], archaeology [41], architecture [35], and urban modeling (e.g. Google Street View); match-moving in augmented reality and cinematography for mixing virtual content and real video [19]; the organization of a collection of photographs with respect to a scene known as Structure-from-Motion [39] (e.g. as pioneered in photo tourism [2]); robotic manipulation [27]; and meteorology from cameras in automobile manufacture and autonomous driving [35]. One key building block of a multiview system is the relative pose estimation of two cameras [26], [47]. A methodology that is dominant in applications is RANSAC [42]. This forms hypotheses from a few randomly selected correspondences in two views, e.g. 5 in calibrated camera pose estimation [38] and 7 in uncalibrated camera pose estimation [44], [45], and validates these hypotheses using the remaining putative correspondences. The chief stated reason for using RANSAC is robustness against outliers, see [4], [7], [37]. The pose of multiple cameras can then be recovered in either a locally incremental [43] or globally averaging manner [30]. This approach has been quite successful in many applications.

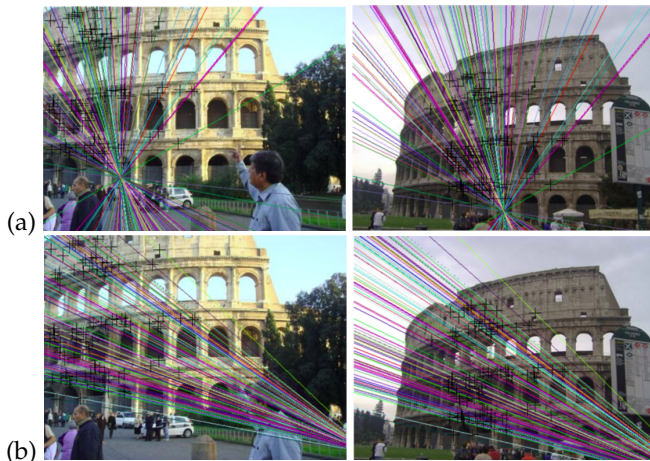


Fig. 1. Typical relative pose estimation can fail catastrophically, even with a large number of correspondences (100 correspondences shown in the figure), all of which are inliers. (a) Ground-truth epipolar geometry. (b) Erroneous estimated epipolar geometry, from the 7-point algorithm and LO-RANSAC [15]. The prime cause of such failure is numerical instability as shown in this paper.

However, there are a non-negligible number of scenarios where the RANSAC-based approach fails, for instance in producing the relative pose between two cameras. As an example, when the number of candidate correspondences drops to say 50 to 100 correspondences, as is the case for images of homogeneous and low textured surfaces, the pose estimation process often fails. It is curious why the estimation should fail, even if only a modicum of correspondences are available: after all RANSAC can select 5 from 50 in  $\binom{50}{5} \approx 2.1$  million combinations for the 5-point problem. Thus there are plenty of veridical correspondences available if the ratio of outliers is low. In an experiment with *no outliers*, either with synthetic data (see Section 7)

• Hongyi Fan and Benjamin Kimia are with the School of Engineering, Brown University, Providence, RI, 02912.

• Joe Kileel is with the Department of Mathematics and Oden Institute for Computational Engineering and Sciences at the University of Texas at Austin, Austin, TX, 78705.

Kimia and Fan were supported in part by NSF awards IIS-1910530 and IIS-2312745. Kileel was supported in part by NSF awards DMS-2309782 and IIS-2312746. Hongyi Fan and Joe Kileel contributed equally to this work. Benjamin Kimia is the corresponding author.

or manually-cleaned real data (see Figure 1), the process can still frequently fail! This is mysterious, unless the role of RANSAC goes beyond weeding out the outliers. Indeed, we argue that a key role for RANSAC is to *stabilize* (or *precondition*) the estimation process, without denying its importance in filtering outliers. We will show that the process of estimating pose from a minimal problem is typically unstable to realistic levels of noise, with a gradation of instability depending on the specific choice of 5 points or 7 points. One role of RANSAC then is to find better-conditioned image data by integrating non-selected correspondences: if a large number of non-selected correspondences agree with the estimate, then the hypothesis is both free of outliers and – perhaps as importantly – it is stable to typical image noise.

Motivated by relative pose estimation, this paper inspects the general issue of instability in minimal problems in multiview geometry. We develop a general framework that connects the conditioning of world scene configurations to the condition number of the inverse of the Jacobian matrix of the forward map, and we relate this to the image data directly (Section 2). Applying the framework, we give condition number formulas for the 5-point and 7-point minimal problems (Propositions 16 and 17). Further, we characterize when the condition number is infinite for the 5- and 7-point minimal problems, both in terms of the world scene (Theorems 18 and 19) and image data (Theorems 20 and 22).

Note that the notion of “critical world scenes” has appeared extensively in the multiview geometry literature already, e.g. [8], [26], [28], [29], [32], [36]. However, the concepts considered previously fundamentally differ from what is studied here. Prior work has focused mostly on non-uniqueness: that is, configurations of cameras and many world points where the image data does not determine the world scene, despite there being more than a minimal set of measurements. By contrast, we consider minimal problems, where usually there are multiple solutions. We quantify the stability of these solutions. Arguably our analysis bears more directly on practice, since RANSAC operates on minimal problems. Further, the results here include characterizations in image space, where the data observations occur, and are not just in terms of the world scene. See Section 5 for more comparison with this part of the literature.

Along with new theory, this paper proposes a computational method to evaluate the stability of a given minimal image correspondence set. The proposal is general, although we only develop it here for relative pose estimation. Our idea is to measure the distance from one image point to a certain “ill-posed curve” on the image plane, computed using the other point correspondences (Section 4.3). The distance is a means of gauging the stability of the data, before solving the minimal problem. We present procedures to compute the ill-posed curve for 5-point and 7-point minimal problems, using methods from numerical and symbolic algebra (Section 6). Experimental results on synthetic and real data show that the measure accurately captures the stability of minimal problems (Section 7). Further we find that in practice, poor conditioning can be a significant challenge for RANSAC and RANSAC exhibits a bias for selecting image data well-separated from the ill-posed curve.

The majority of the content in this paper has been published in a conference paper [21]. In this version, we develop

a new method to compute the ill-posed curve for the 7-point problem, which is  $100\times$  faster than before and now suitable for real-time computations (Section 6.2). We also expand the framework in Section 3, by introducing a condition number associated to image data and providing the new Section 3.4 which describes a tool from computational algebra. This makes the framework more readily usable for other minimal problems. Further, we compare our instability analysis to the traditional critical configurations analysis found in the literature, in the newly-added Section 5. Also, Section 2 is revamped through the addition of results on the quotient manifold construction we use to formalized world scenes; this makes parts of the paper more rigorous. Additionally, new numerical experiments are in Section 7, which better connect our theory to common practice. Finally, throughout the paper the presentation is substantially improved.

## 2 MINIMAL PROBLEMS FOR RELATIVE POSE ESTIMATION

We review the classic 5- and 7-point minimal problems for relative pose estimation, which serve as key motivating examples. We formulate the problems in a way that fits into the general framework in Section 3. Terms appearing in bold will be reused there.

### 2.1 Essential matrices and the 5-point problem

This is the minimal problem for computing the essential matrix between two calibrated cameras given 5 point matches.

We define world scenes to be tuples of 2 calibrated cameras and 5 world points up to changes of world coordinates. This is formalized using the quotient manifold theorem [34, Thm. 21.10]. Namely, let  $\mathcal{W}$  be the **world scene space**:

$$\begin{aligned} \mathcal{W} &= \{(P, \bar{P}, \Gamma_1, \dots, \Gamma_5) \in \mathcal{C}^{\times 2} \times (\mathbb{R}^3)^{\times 5} : \ker(P) \neq \ker(\bar{P}), \\ &\quad (P(\Gamma_i; 1))_3 \neq 0 \text{ and } (\bar{P}(\Gamma_i; 1))_3 \neq 0 \text{ for all } i\} / G \\ &= \{(P, \bar{P}, \Gamma_1, \dots, \Gamma_5) \bmod G\}. \end{aligned} \quad (1)$$

Here

$\mathcal{C} = \{P \in \mathbb{P}(\mathbb{R}^{3 \times 4}) : \exists \mathbf{R} \in \text{SO}(3), \mathbf{T} \in \mathbb{R}^3 \text{ s.t. } P = (\mathbf{R} \ \mathbf{T})\}$ , consists of calibrated cameras, and

$$\Gamma_i \in \mathbb{R}^3 \quad (i = 1, \dots, 5)$$

are the 3D points. Also

$$\begin{aligned} G &= \{g \in \mathbb{P}(\mathbb{R}^{4 \times 4}) : \exists \mathbf{R} \in \text{SO}(3), \mathbf{T} \in \mathbb{R}^3, \lambda \in \mathbb{R} \setminus \{0\} \\ &\quad \text{s.t. } g = \begin{pmatrix} \mathbf{R} & \mathbf{T} \\ 0 & \lambda \end{pmatrix}\} \end{aligned}$$

is the group of world transformations preserving calibration, which acts on  $\mathcal{C}^{\times 2} \times (\mathbb{R}^3)^{\times 5}$  via

$$g \cdot (P, \bar{P}, \Gamma_1, \dots) := (Pg^{-1}, \bar{P}g^{-1}, \frac{1}{\lambda}(\mathbf{R}\Gamma_1 + \mathbf{T}), \dots). \quad (2)$$

Altogether  $\mathcal{W}$  consists of pairs of calibrated cameras with distinct centers and world points whose images are finite, up to change of world coordinates.

**Proposition 1.** The action of  $G$  on the subset of  $\mathcal{C}^{\times 2} \times (\mathbb{R}^3)^{\times 5}$  in (1) is smooth, free and proper. Therefore the quotient  $\mathcal{W}$  is canonically a smooth manifold of dimension 20.

The proposition is proven in the appendices.

The benefit of the quotient space construction is that it is intrinsic. This makes it clear we may use any coordinate system and no conclusions will be affected. That said, we use:

**Lemma 2.** Let  $\mathcal{U} = \{(\mathbf{R}, \hat{\mathbf{T}}, \Gamma_1, \dots, \Gamma_5)\}$  be the open subset of  $\text{SO}(3) \times \mathbb{S}^2 \times (\mathbb{R}^3)^{\times 5}$  where  $(\Gamma_i)_3 \neq 0$  and  $(\mathbf{R}\Gamma_i + \hat{\mathbf{T}})_3 \neq 0$  for  $i = 1, \dots, 5$ . Then the map  $\mathcal{U} \rightarrow \mathcal{W}$  sending  $(\mathbf{R}, \hat{\mathbf{T}}, \Gamma_1, \dots, \Gamma_5)$  to  $((I \ 0), (\mathbf{R} \ \hat{\mathbf{T}}), \Gamma_1, \dots, \Gamma_5)$  is a smooth double cover of  $\mathcal{W}$  in the sense of [34, Ch. 4].

The lemma is proven in the appendices. The map identifies  $(\mathbf{R}, \hat{\mathbf{T}}, \Gamma_1, \dots, \Gamma_5)$  and  $(\mathbf{R}, -\hat{\mathbf{T}}, -\Gamma_1, \dots, -\Gamma_5)$ , which is a well-known ambiguity [26, Sec. 9.6.2].

Continuing, define  $\mathcal{X}$  as the relevant **image data space**:

$$\mathcal{X} = (\mathbb{R}^2 \times \mathbb{R}^2)^{\times 5} = \{(\gamma_1, \bar{\gamma}_1), \dots, (\gamma_5, \bar{\gamma}_5)\}. \quad (3)$$

This consists of 5-tuples of image point pairs. Here

$$\gamma_i \in \mathbb{R}^2 \quad \text{and} \quad \bar{\gamma}_i \in \mathbb{R}^2 \quad (i = 1, \dots, 5)$$

denotes corresponding points in the two images.

Next, define  $\mathcal{Y}$  to be the relevant **output space**:

$$\begin{aligned} \mathcal{Y} &= \{E \in \mathbb{P}(\mathbb{R}^{3 \times 3}) : E \text{ is an essential matrix}\} \\ &= \{E \in \mathbb{P}(\mathbb{R}^{3 \times 3}) : 2EE^\top E - \text{tr}(EE^\top)E = 0, \det(E) = 0\} \\ &= \{E \in \mathbb{P}(\mathbb{R}^{3 \times 3}) : \sigma_1(E) = \sigma_2(E) > \sigma_3(E) = 0\}. \end{aligned} \quad (4)$$

This consists of the quantities of interest that we solve for in the minimal problem, *i.e.* essential matrices. Here essential matrices are characterized in terms of the vanishing of ten cubic equations [17], or via singular values.

Define  $\Phi$  as the **forward map** from world scenes to image data:

$$\Phi(\mathbf{R}, \hat{\mathbf{T}}, \Gamma_1, \dots, \Gamma_5) = ((\gamma_1, \bar{\gamma}_1), \dots, (\gamma_5, \bar{\gamma}_5)), \quad (5)$$

for  $\gamma_i = \pi(\Gamma_i)$  and  $\bar{\gamma}_i = \pi(\mathbf{R}\Gamma_i + \hat{\mathbf{T}})$

where  $\pi(x, y, z) = (x/z, y/z)$  is orthographic projection.

Replacing  $(\mathbf{R}, \hat{\mathbf{T}}, \Gamma_1, \dots, \Gamma_5)$  by  $(\mathbf{R}, -\hat{\mathbf{T}}, -\Gamma_1, \dots, -\Gamma_5)$  gives the same image. Therefore  $\Phi$  is well-defined on  $\mathcal{W}$ .

Define  $\Psi$  as the relevant **output map** from world scenes to the quantities of interest:

$$\Psi(\mathbf{R}, \hat{\mathbf{T}}, \Gamma_1, \dots, \Gamma_5) = E = [\hat{\mathbf{T}}]_{\times} \mathbf{R} \in \mathbb{P}(\mathbb{R}^{3 \times 3}). \quad (6)$$

Here  $[\hat{\mathbf{T}}]_{\times} \in \mathbb{R}^{3 \times 3}$  is the skew symmetric matrix representation of taking cross product with a vector  $\hat{\mathbf{T}} \in \mathbb{R}^3$  [26, Sec. 9.6].

At last, the **minimal problem** is to compute  $\Psi(\Phi^{-1}(\cdot))$  for different instances of image data in  $\mathcal{X}$ . The output is up to 10 essential matrices in  $\mathcal{Y}$ . [26, Part II] shows these are the essential matrices satisfying the **epipolar constraints**:

$$(\bar{\gamma}_i; 1)^\top E (\gamma_i; 1) = 0 \quad \text{for } i = 1, \dots, 5. \quad (7)$$

They can be found by solvers based on computing the real roots of a degree 10 univariate polynomial [38]. In this paper the questions are: How sensitive are the essential matrices to perturbations in the image data? Which world scenes map to ill-conditioned image data? How do we detect directly from the image data that a problem instance is poorly conditioned? The answers are in Section 4.

## 2.2 Fundamental matrices and the 7-point problem

This is the minimal problem for computing the fundamental matrix between two uncalibrated cameras given 7 point matches.

Define  $\mathcal{W}$  as the **world scene space** as a quotient:

$$\begin{aligned} \mathcal{W} &= \{(P, \bar{P}, \tilde{\Gamma}_1, \dots, \tilde{\Gamma}_7) \in \mathcal{C}^{\times 2} \times (\mathbb{P}_{\mathbb{R}}^3)^{\times 7} : \ker(P) \neq \ker(\bar{P}), \\ &\quad (P\tilde{\Gamma}_i)_3 \neq 0 \text{ and } (\bar{P}\tilde{\Gamma}_i)_3 \neq 0 \text{ for all } i\} / \text{PGL}(4) \\ &= \{(P, \bar{P}, \tilde{\Gamma}_1, \dots, \tilde{\Gamma}_7) \text{ mod PGL}(4)\}. \end{aligned} \quad (8)$$

Here

$$\mathcal{C} = \{P \in \mathbb{P}(\mathbb{R}^{3 \times 4}) : \text{rank}(P) = 3\}$$

are projective cameras and  $\tilde{\Gamma}_i \in \mathbb{P}_{\mathbb{R}}^3$  are projective world points. Also,

$$\text{PGL}(4) = \{g \in \mathbb{P}(\mathbb{R}^{4 \times 4}) : \det(g) \neq 0\}$$

is the group of projective world transformations, acting on  $\mathcal{C}^{\times 2} \times (\mathbb{P}_{\mathbb{R}}^3)^{\times 7}$  via

$$g \cdot (P, \bar{P}, \tilde{\Gamma}_1, \dots, \tilde{\Gamma}_7) = (Pg^{-1}, \bar{P}g^{-1}, g\tilde{\Gamma}_1, \dots, g\tilde{\Gamma}_7). \quad (9)$$

Altogether  $\mathcal{W}$  consists pairs of projective cameras with distinct centers and world points whose images are finite, up to change of world coordinates.

**Proposition 3.** The action of  $\text{PGL}(4)$  on the subset of  $\mathcal{C}^{\times 2} \times (\mathbb{P}_{\mathbb{R}}^3)^{\times 7}$  in (8) is smooth, free and proper. Therefore the quotient  $\mathcal{W}$  is canonically a smooth manifold of dimension 28.

The proposition is proven in the appendices.

**Lemma 4.** Let  $\mathbf{M}(b) = \begin{pmatrix} 1 & b_1 & b_2 & b_3 \\ b_4 & b_5 & b_6 & b_7 \\ 0 & 0 & 0 & 1 \end{pmatrix}$  for  $b \in \mathbb{R}^7$  and

$\tilde{\Gamma}_i = (\Gamma_i; 1)$  for  $\Gamma_i \in \mathbb{R}^3$ . Let  $\mathcal{U} = \{(b, \Gamma_1, \dots, \Gamma_7)\}$  be the open subset of  $\mathbb{R}^7 \times (\mathbb{R}^3)^{\times 7}$  where  $\text{rank}(\mathbf{M}(b)) = 3$ ,  $(\Gamma_i)_3 \neq 0$  and  $(\mathbf{M}(b)\tilde{\Gamma}_i)_3 \neq 0$  for  $i = 1, \dots, 5$ . Then the map from  $\mathcal{U}$  to  $\mathcal{W}$  sending  $(b, \Gamma_1, \dots, \Gamma_7)$  to  $((I \ 0), \mathbf{M}(b), \tilde{\Gamma}_1, \dots, \tilde{\Gamma}_7) \text{ mod PGL}(4)$  is a smooth parameterization of an open dense subset of  $\mathcal{W}$ . Further, suppose in  $\mathbf{M}$  we swap the third row with the first or second row and/or the first column with the second or third column. In  $\tilde{\Gamma}_i$ , we swap the fourth entry with one of the first three. Then these maps form an atlas for  $\mathcal{W}$ .

The lemma is proven in the appendices. It gives concrete coordinates for projective world scenes.

Continuing, define  $\mathcal{X}$  as the **image data space**:

$$\mathcal{X} = (\mathbb{R}^2 \times \mathbb{R}^2)^{\times 7} = \{(\gamma_1, \bar{\gamma}_1), \dots, (\gamma_7, \bar{\gamma}_7)\}, \quad (10)$$

consisting of 7-tuples of image point pairs.

Let  $\mathcal{Y}$  be the relevant **output space**:

$$\begin{aligned} \mathcal{Y} &= \{F \in \mathbb{P}(\mathbb{R}^{3 \times 3}) : F \text{ is a fundamental matrix}\} \\ &= \{F \in \mathbb{P}(\mathbb{R}^{3 \times 3}) : \text{rank}(F) = 2\}. \end{aligned} \quad (11)$$

Let  $\Phi$  be **forward map** from world scenes to image data:

$$\Phi(P, \bar{P}, \tilde{\Gamma}_1, \dots, \tilde{\Gamma}_7) = ((\gamma_1, \bar{\gamma}_1), \dots, (\gamma_7, \bar{\gamma}_7)), \quad (12)$$

for  $\gamma_i = \pi(P\tilde{\Gamma}_i)$  and  $\bar{\gamma}_i = \pi(\bar{P}\tilde{\Gamma}_i)$

where  $\pi(x, y, z) = (x/z, y/z)$ .

Note  $P\tilde{\Gamma}_i$  and  $\bar{P}\tilde{\Gamma}_i$  are well-defined on  $\mathcal{W}$ , as  $g^{-1}$  and  $g$  cancel out in the action (9).

Define  $\Psi$  as the **output map** from world scenes to the quantities of interest:

$$\Psi(P, \bar{P}, \tilde{\Gamma}_1, \dots, \tilde{\Gamma}_7) = \text{fund. matrix of } P, \bar{P} \in \mathbb{P}(\mathbb{R}^{3 \times 3}). \quad (13)$$

Explicitly (13) equals  $F \in \mathbb{P}(\mathbb{R}^{3 \times 3})$  such that  $F_{ij} = (-1)^{i+j} \det \begin{pmatrix} P_j \\ \bar{P}_i \end{pmatrix}$  where  $P_j$  denotes  $P$  with the  $j$ th row dropped and similarly for  $\bar{P}_i$ .

The **minimal problem** is to compute:

$$\Psi(\Phi^{-1}(\cdot)) \quad (14)$$

for various instances of image data in  $\mathcal{X}$ . The output is up to 3 real fundamental matrices in  $\mathcal{Y}$ . [26, Part II] implies these are the fundamental matrices satisfying the **epipolar constraints**:

$$(\bar{\gamma}_i; 1)^\top F(\gamma_i; 1) = 0 \quad \text{for } i = 1, \dots, 7. \quad (15)$$

The solutions can be found by computing the real roots of a cubic univariate polynomial [26, Sec. 11.1.2]. The questions we want to answer are the same as in Section 2.1: How sensitive are the outputs to noise in the input? Which world scenes and image data instances are ill-posed? Answers are in Section 4.

### 3 GENERAL FRAMEWORK

In this section we present a general framework for analyzing instabilities in minimal problems in multiview geometry.

#### 3.1 Spaces and maps

In general, minimal problems involve three spaces. Typically, they are all smooth manifolds:

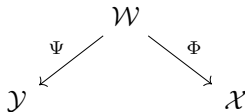
- $\mathcal{W}$ , the **world scene space**;
- $\mathcal{X}$ , the **image data space**;
- $\mathcal{Y}$ , the **output space**.

To quantify instability, distances are needed on  $\mathcal{X}$  (the input space) and  $\mathcal{Y}$  (the output space). We adopt the formalism of Burgisser and Cucker [12], and assume  $\mathcal{X}$  and  $\mathcal{Y}$  are endowed with Riemannian metrics. Let  $T(\mathcal{X}, \cdot)$  denote a tangent spaces to  $\mathcal{X}$ ,  $\langle \cdot, \cdot \rangle$  its inner product, and  $d_{\mathcal{X}}(\cdot, \cdot)$  the geodesic distance on  $\mathcal{X}$ , and likewise for other spaces. In the appendix, we list the tangent spaces and relevant Riemannian metrics for the manifolds from Section 2.

Continuing, minimal problems feature two smooth maps:

- $\Phi$ , the **forward map**;
- $\Psi$ , the **output map**.

These connect the spaces as follows:



The **minimal problem** is to compute:

$$\Psi(\Phi^{-1}(\cdot)) \quad (16)$$

for different image data inputs  $x \in \mathcal{X}$ . “Minimal” refers to the case where the output (16) is a finite set for almost all  $x$ . To ensure this, following [20] we assume further that  $\mathcal{W}, \mathcal{X}, \mathcal{Y}$  are quasi-projective irreducible connected real algebraic varieties with

$$\dim(\mathcal{W}) = \dim(\mathcal{X}).$$

Additionally, we assume  $\Phi$  and  $\Psi$  are dominant algebraic maps. These assumptions guarantee (16) is a finite set for almost all  $x$  and is nonempty for  $x$  in a positive Lebesgue-measure subset of  $\mathcal{X}$  [25]. Roughly, the conditions just say that all spaces and maps can be described by polynomial equations, as commonly the case in multiview geometry.

#### 3.2 Definition of condition number

Let  $\mathcal{M} = (\mathcal{W}, \mathcal{X}, \mathcal{Y}, \Phi, \Psi)$  be a minimal problem. In general, condition numbers quantify the worst-case first-order amplification of error from the input to the output [12, Sec. O.2]. For minimal problems we attach condition numbers to world scenes and image data.

**Definition 5.** Let  $w \in \mathcal{W}$ . Define the **condition number of  $\mathcal{M}$  associated to  $w$**  by

$$\text{cond}(\mathcal{M}, w) := \sigma_{\max}(D\Psi(w) \circ D\Phi(w)^{-1}) \quad (17)$$

if  $D\Phi(w)$  is invertible, and  $\text{cond}(\mathcal{M}, w) := \infty$  else.

We explain the notation. Here  $D\Phi(w) : T(\mathcal{W}, w) \rightarrow T(\mathcal{X}, \Phi(w))$  and  $D\Psi(w) : T(\mathcal{W}, w) \rightarrow T(\mathcal{Y}, \Psi(w))$  denote differentials [34, Sec. 3]. The right-hand side of (17) is the maximum singular value [23] with respect to the Riemannian metrics on  $\mathcal{X}$  and  $\mathcal{Y}$ . Concretely, we need to express the differentials as Jacobian matrices using orthonormal bases on  $T(\mathcal{X}, \Phi(w))$  and  $T(\mathcal{Y}, \Psi(w))$  and any basis on  $T(\mathcal{W}, w)$ . Then  $\text{cond}(\mathcal{M}, w)$  is the maximum singular value of the matrix product in (17). We use the maximum singular value rather than the ratio of the maximum to minimum singular values to capture the amplification of *absolute* errors rather than *relative* errors, see [12, Sec. 14.1].

**Lemma 6.** Let  $w \in \mathcal{W}$  and assume  $D\Phi(w)$  is invertible. Then there exist open neighborhoods  $\mathcal{X}_0 \subseteq \mathcal{X}$  of  $x = \Phi(w)$  and  $\mathcal{W}_0 \subseteq \mathcal{W}$  of  $w$  such that there is a unique continuous map  $\Theta : \mathcal{X}_0 \rightarrow \mathcal{W}_0$  with  $\Theta(x) = w$  and  $\Phi \circ \Theta = \text{id}_{\mathcal{X}}$ . Moreover,  $\Theta$  is smooth, and

$$D(\Psi \circ \Theta)(x) = D\Psi(w) \circ D\Phi(w)^{-1}. \quad (18)$$

**Proof:** This is immediate from the inverse function theorem and chain rule [34, Thm. 4.5 and Prop. 3.6].  $\square$

This shows Definition 5 quantifies the most that the output associated with  $w$  can change, as  $x = \Phi(w)$  is perturbed.

**Definition 7.** Let  $x \in \mathcal{X}$ . Define the **condition number of  $\mathcal{M}$  associated to  $x$**  by

$$\text{cond}(\mathcal{M}, x) := \max\{\text{cond}(\mathcal{M}, w) : \Phi(w) = x\}. \quad (19)$$

Again by Lemma 6, Definition 7 captures the most that *any* of the outputs associated to  $x$  can change, as  $x$  is perturbed.

It should be emphasized that directly computing (19) is no easier than solving the minimal problem (16) itself for  $x$ , because all world scenes satisfying  $\Phi(w) = x$  are involved.

However, there is a method to *precompute* an approximation to  $\text{cond}(\mathcal{M}, x)$  without solving  $\mathcal{M}$ , explained below (Sections 3.4 and 6).

### 3.3 Definition of ill-posed locus

The world scenes and image data with infinite condition number play important roles in instability analysis.

**Definition 8.** Define the **ill-posed locus of  $\mathcal{M}$  in  $\mathcal{W}$**  by

$$\text{ill}(\mathcal{M}, \mathcal{W}) := \{w \in \mathcal{W} : D\Phi(w) \text{ is rank-deficient}\}. \quad (20)$$

**Definition 9.** Define the **ill-posed locus of  $\mathcal{M}$  in  $\mathcal{X}$**  by

$$\text{ill}(\mathcal{M}, \mathcal{X}) := \Phi(\text{ill}(\mathcal{M}, \mathcal{W})). \quad (21)$$

Ill-posed loci and their neighborhoods are danger zones for minimal problems. If  $w$  lies *exactly* in  $\text{ill}(\mathcal{M}, \mathcal{W})$ , the output associated with  $w$  has unbounded error compared to the error in the input, as  $x = \Phi(w)$  is perturbed. Similarly if  $x \in \text{ill}(\mathcal{M}, \mathcal{X})$ , one of the outputs associated to  $x$  suffers unbounded error amplification. Meanwhile at world scenes or image data lying *close* to the ill-posed loci, the condition number is finite but very large, which is still problematic.

We propose the **reciprocal distances** to the ill-posed loci:

$$1 / d_{\mathcal{W}}(w, \text{ill}(\mathcal{M}, \mathcal{W})) \quad \text{and} \quad 1 / d_{\mathcal{X}}(x, \text{ill}(\mathcal{M}, \mathcal{X})) \quad (22)$$

as proxies for the conditions numbers

$$\text{cond}(\mathcal{M}, w) \quad \text{and} \quad \text{cond}(\mathcal{M}, x),$$

respectively. This approximation is known to be exact in some cases. For example, in [18, Sec. 3] Demmel studied matrix inversion. Given a square matrix, he proved that its reciprocal Frobenius distance to rank-deficient matrices equals the relevant condition number.

### 3.4 Tool from computational algebra

Many minimal problems can be recast in terms of epipolar constraints, which are linear in the output variable. When this is the case, a tool from computational algebra can be applied to instability analysis.

Assume  $\mathcal{Y} \subseteq \mathbb{P}_{\mathbb{R}}^n$  for some  $n$ , and let  $\dim(\mathcal{Y}) = d$ .

**Definition 10.** Given  $\mathcal{M} = (\mathcal{W}, \mathcal{X}, \mathcal{Y}, \Phi, \Psi)$ . Say an algebraic map  $\mathbf{L} : \mathcal{X} \rightarrow \mathbb{P}(\mathbb{R}^{k \times (n+1)})$  is an **epipolar map for  $\mathcal{M}$**  if

$$\Psi(\Phi^{-1}(x)) = \mathcal{Y} \cap \ker \mathbf{L}(x) \quad \text{for all } x \in \mathcal{X}, \text{ and}$$

$$\dim(\ker \mathbf{L}(x)) = n - d \text{ for Zariski-generic } x \in \mathcal{X}. \quad (23)$$

Here  $k$  is some fixed integer,  $\mathbf{L}(x)$  is a  $k \times (n+1)$  matrix and the right kernel  $\ker \mathbf{L}(x)$  is a linear subspace of  $\mathbb{P}_{\mathbb{R}}^n$ .

**Example 11.** In the 5-point problem (Section 2.1), we have  $n = 8$ ,  $d = 5$  and  $k = 5$ . The epipolar constraints are encoded by the  $5 \times 9$  matrix  $\mathbf{L}((\gamma_1, \bar{\gamma}_1), \dots, (\gamma_5, \bar{\gamma}_5))$ , whose  $i$ th row is the vectorization of  $[\gamma_i; 1] \otimes [\bar{\gamma}_i; 1]$ . Similarly, the 7-point problem has an epipolar map.

If there exists an epipolar map, then the minimal problem has a nice geometric interpretation: its output is the intersection of  $\mathcal{Y}$  with a varying linear space in  $\mathbb{P}_{\mathbb{R}}^n$  of complementary dimension.

**Definition 12.** Define the **discriminant of  $\mathcal{M}$  and  $\mathbf{L}$  in  $\mathcal{X}$**  as

$$\text{disc}(\mathcal{M}, \mathbf{L}) := \{x \in \mathcal{X} : \text{rank}(\mathbf{L}(x)) < d \text{ or } \mathcal{Y} \cap \ker \mathbf{L}(x) \text{ is not a transversal intersection}\}. \quad (24)$$

Recall that  $\mathcal{Y} \cap \ker \mathbf{L}(x) \subseteq \mathbb{P}_{\mathbb{R}}^n$  is a transversal intersection if for all  $y \in \mathcal{Y} \cap \ker \mathbf{L}(x)$  we have  $T(\mathcal{Y}, y) + T(\ker \mathbf{L}(x), y) = T(\mathbb{P}_{\mathbb{R}}^n, y)$ , see [34, Sec. 6]. Therefore the discriminant captures partial tangencies, or “double roots”.

It turns out that there is a characterization of this discriminant, due to Sturmfels.

**Theorem 13.** [46, Thm. 1.1] There exists a nonzero polynomial  $\mathbf{P}_{\mathcal{Y}}$  in the  $\binom{n+1}{d}$  Plücker coordinates for codimension- $d$  linear subspaces of  $\mathbb{P}_{\mathbb{R}}^n$ , depending only on  $\mathcal{Y}$ , such that

$$x \in \text{disc}(\mathcal{M}, \mathbf{L}) \implies \mathbf{P}_{\mathcal{Y}}(\ker \mathbf{L}(x)) = 0. \quad (25)$$

Furthermore, the degree of  $\mathbf{P}_{\mathcal{Y}}$  is  $2p + 2g - 2$  where  $p$  and  $g$  are the degree and sectional genus of the complex Zariski closure  $\mathcal{Y}_{\mathbb{C}} \subseteq \mathbb{P}_{\mathbb{C}}^n$  of  $\mathcal{Y}$ , assuming  $p \geq 2$  and the singular locus of  $\mathcal{Y}_{\mathbb{C}}$  has codimension at least 2.

We review Plücker coordinates in the appendix. For details on the other notions from algebraic geometry (not needed here), see [46] and references therein.

The discriminant is closely related to the ill-posed locus.

**Lemma 14.** Let  $x \in \mathcal{X} \setminus \text{disc}(\mathcal{M}, \mathbf{L})$  and  $y \in \mathcal{Y} \cap \ker \mathbf{L}(x)$ . Then there exist open neighborhoods  $\mathcal{X}_0 \subseteq \mathcal{X}$  of  $x$  and  $\mathcal{Y}_0 \subseteq \mathcal{Y}$  of  $y$  such that for all  $x' \in \mathcal{X}_0$  the intersection  $\mathcal{Y}_0 \cap \ker \mathbf{L}(x')$  is a singleton. Further, the map  $f : \mathcal{X}_0 \rightarrow \mathcal{Y}_0$  sending  $x'$  to  $\mathcal{Y}_0 \cap \ker \mathbf{L}(x')$  is smooth.

**Proof:** This follows from the implicit function theorem [34, Thm. C.40]. Also see [11].  $\square$

**Proposition 15.** Assume  $\mathcal{M}$  and  $\mathbf{L}$  satisfy the following **smooth lifting property**: For all  $x \in \mathcal{X} \setminus \text{disc}(\mathcal{M}, \mathbf{L})$ ,  $y \in \mathcal{Y} \cap \ker \mathbf{L}(x)$  and  $w \in \Phi^{-1}(x) \cap \Psi^{-1}(y)$ , we can take  $\mathcal{X}_0$  and  $\mathcal{Y}_0$  in Lemma 14 such that there further exists a smooth map  $h : \mathcal{X}_0 \rightarrow \mathcal{W}$  such that  $h(x) = w$ ,  $\Psi \circ h = f$  and  $\Phi \circ h = \text{id}_{\mathcal{X}_0}$ . Then it holds

$$\text{ill}(\mathcal{M}, \mathcal{X}) \subseteq \text{disc}(\mathcal{M}, \mathbf{L}). \quad (26)$$

**Proof:** Take  $x \in \mathcal{X} \setminus \text{disc}(\mathcal{M}, \mathbf{L})$ . We need to show  $x \in \mathcal{X} \setminus \text{ill}(\mathcal{M}, \mathcal{X})$ . Let  $w \in \Phi^{-1}(x) \in \mathcal{W}$  and  $y = \Psi(w)$ . By the first line of (23),  $y \in \mathcal{Y} \cap \ker \mathbf{L}(x)$ . Clearly,  $w \in \Phi^{-1}(x) \cap \Psi^{-1}(y)$ . So the smooth lifting property applies. From  $\Phi \circ h = \text{id}_{\mathcal{X}_0}$  and  $h(x) = w$ , the chain rules gives  $D\Phi(w) \circ Dh(x) = \text{id}$ . In particular,  $D\Phi(w)$  is invertible. Since  $w \in \Phi^{-1}(x)$  was arbitrary,  $x \notin \text{ill}(\mathcal{M}, \mathcal{X})$  by Definition 9.  $\square$

Putting Theorem 13 and Proposition 15 together,

$$x \in \text{ill}(\mathcal{M}, \mathcal{X}) \implies \mathbf{P}_{\mathcal{Y}}(\ker \mathbf{L}(x)) = 0$$

if the property in Proposition 15 holds. Importantly, we can precompute an approximation to  $\text{cond}(\mathcal{M}, x)$ , by estimating the reciprocal distance of  $x$  to the zero set of  $\mathbf{P}_{\mathcal{Y}}(\ker \mathbf{L}(\cdot))$ .

## 4 MAIN THEORETICAL RESULTS

We apply the framework to analyze the stability of the 5- and 7-point minimal problems from Section 2.

#### 4.1 Condition number formulas

It is a matter of computation to obtain explicit condition number formulas. We do this in terms of the Euclidean distance on  $\mathcal{X}$ , and the metric inherited from  $\mathbb{P}(\mathbb{R}^{3 \times 3})$  on  $\mathcal{Y}$ .

**Proposition 16.** Consider the 5-point problem from Section 2.1. Let  $w = (\mathbf{R}, \hat{\mathbf{T}}, \Gamma_1, \dots, \Gamma_5)$  be a world scene, written as in Lemma 2. If finite, then  $\text{cond}(\mathcal{M}, w)$  equals the largest singular value of an explicit  $5 \times 20$  matrix. The matrix naturally factors as a  $5 \times 20$  matrix multiplied by a  $20 \times 20$  matrix.

**Sketch:** By Definition 5, if it is finite then

$$\text{cond}(\mathcal{M}, w) = \sigma_{\max}(D\Psi(w) \circ D\Phi(w)^{-1}) \quad (27)$$

where  $\Phi$  and  $\Psi$  are given by (5) and (6). We factor the forward map as

$$\Phi = \Phi_2 \circ \Phi_1,$$

where  $\Phi_1 : \mathcal{U} \subseteq \text{SO}(3) \times \mathbb{S}^2 \times (\mathbb{R}^3)^{\times 5} \rightarrow (\mathbb{R}^3 \times \mathbb{R}^3)^{\times 5}$  is

$$\begin{aligned} \Phi_1(\mathbf{R}, \hat{\mathbf{T}}, \Gamma_1, \dots, \Gamma_5) = \\ ((\Gamma_1, \mathbf{R}\Gamma_1 + \hat{\mathbf{T}}), \dots, (\Gamma_5, \mathbf{R}\Gamma_5 + \hat{\mathbf{T}})), \end{aligned} \quad (28)$$

and  $\Phi_2 : (\mathbb{R}^3 \times \mathbb{R}^3)^{\times 5} \dashrightarrow (\mathbb{R}^2 \times \mathbb{R}^2)^{\times 5}$  is

$$\begin{aligned} \Phi_2((\Gamma_1, \bar{\Gamma}_1), \dots, (\Gamma_5, \bar{\Gamma}_5)) = \\ ((\pi(\Gamma_1), \pi(\bar{\Gamma}_1)), \dots, (\pi(\Gamma_5), \pi(\bar{\Gamma}_5))) \end{aligned} \quad (29)$$

where the broken arrow indicates a rational map. By the chain rule,

$$D\Phi = D\Phi_2 \circ D\Phi_1. \quad (30)$$

Here  $\Phi_1$  is multi-affine in  $\Gamma_i, \mathbf{R}, \hat{\mathbf{T}}$ , while  $\Phi_2 = (\pi \times \pi)^{\times 5}$ , so they are easily differentiated. See the appendices for explicit expressions, with respect to an orthonormal basis of  $T(\mathcal{X}, x)$ . Meanwhile  $\Psi$  is  $(\mathbf{R}, \hat{\mathbf{T}}, \Gamma_1, \dots, \Gamma_7) \mapsto [\hat{\mathbf{T}}]_{\times} \mathbf{R}$ . See the appendices for its Jacobian matrix with respect to an orthonormal basis for  $T(\mathcal{Y}, y)$ . Inserting these into (27) finishes the proof.  $\square$

**Proposition 17.** Consider the 7-point problem from Section 2.2. Let  $w = (b, \Gamma_1, \dots, \Gamma_7)$  be a world scene, written as in Lemma 4. If finite, then  $\text{cond}(\mathcal{M}, w)$  equals the largest singular value of an explicit  $7 \times 28$  matrix. The matrix naturally factors as a  $7 \times 28$  matrix multiplied by a  $28 \times 28$  matrix.

**Sketch:** If the condition number is finite, then

$$\text{cond}(\mathcal{M}, w) = \sigma_{\max}(D\Psi(w) \circ D\Phi(w)^{-1}) \quad (31)$$

where  $\Phi$  and  $\Psi$  are given by (12) and (13). We factor

$$\Phi = \Phi_2 \circ \Phi_1,$$

where  $\Phi_1 : \mathcal{U} \subseteq \mathbb{R}^7 \times (\mathbb{R}^3)^{\times 7} \rightarrow (\mathbb{R}^3 \times \mathbb{R}^3)^{\times 7}$  is

$$\Phi_1(b, \Gamma_1, \dots, \Gamma_7) = ((\Gamma_1, \mathbf{M}(b)\bar{\Gamma}_1), \dots, (\Gamma_7, \mathbf{M}(b)\bar{\Gamma}_7)), \quad (32)$$

and  $\Phi_2 : (\mathbb{R}^3 \times \mathbb{R}^3)^{\times 7} \dashrightarrow (\mathbb{R}^2 \times \mathbb{R}^2)^{\times 7}$  is

$$\begin{aligned} \Phi_2((\Gamma_1, \bar{\Gamma}_1), \dots, (\Gamma_7, \bar{\Gamma}_7)) = \\ ((\pi(\Gamma_1), \pi(\bar{\Gamma}_1)), \dots, (\pi(\Gamma_7), \pi(\bar{\Gamma}_7))). \end{aligned} \quad (33)$$

Using the chain rule and an orthonormal basis for  $T(\mathcal{X}, x)$ , we compute  $D\Phi$  in the appendices. We also compute the Jacobian  $D\Psi$  with respect to an orthonormal basis for  $T(\mathcal{Y}, y)$ .  $\square$

#### 4.2 Ill-posed world scenes

We derive geometric characterizations of ill-posed world scenes. The results are in terms of the existence of certain quadric surfaces in  $\mathbb{R}^3$ .

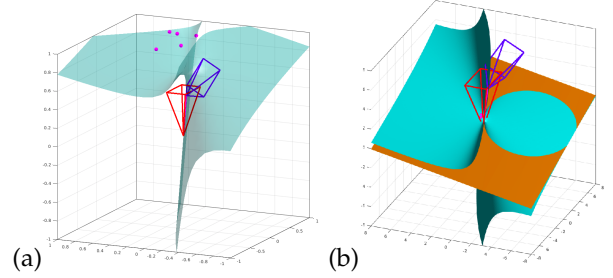


Fig. 2. An ill-posed world scene in the calibrated case. Red and blue pyramids represent two cameras. Magenta points represent five world points. The green surface is a quadric surface satisfying the conditions in Theorem 18. The view (b) shows an orange plane perpendicular to the baseline whose intersection with the quadric surface is a circle.

**Theorem 18.** Consider the 5-point problem from Section 2.1.

Let  $w = (\mathbf{R}, \hat{\mathbf{T}}, \Gamma_1, \dots, \Gamma_5) \in \mathcal{W}$  be a world scene, written as in Lemma 2. Then  $w \in \text{ill}(\mathcal{M}, \mathcal{W})$  if and only if there exists a quadric surface  $\mathcal{Q}$  in  $\mathbb{R}^3$  such that:

- $\Gamma_i \in \mathcal{Q}$  for each  $i = 1, \dots, 5$ ;
- $\ell \subseteq \mathcal{Q}$  where  $\ell = \text{span}(\mathbf{R}^T \hat{\mathbf{T}})$  is the baseline through the two camera centers;
- $\mathcal{N} \cap \mathcal{Q}$  is a circle for each affine plane  $\mathcal{N}$  in  $\mathbb{R}^3$  normal to  $\ell$ .

**Sketch:** Let  $\delta w = (\delta \mathbf{R}, \delta \hat{\mathbf{T}}, \delta \Gamma_1, \dots, \delta \Gamma_5) \in T(\mathcal{W}, w)$ . We need to characterize the world scenes  $w$  such that

$$D\Phi(w)(\delta w) = 0 \quad (34)$$

admits a nonzero solution in  $\delta w$ . In the appendices, we show there exists an invertible change of coordinates exists so that without loss of generality  $\mathbf{R} = I$  and  $\hat{\mathbf{T}} = \mathbf{e}_3$ . Recall  $D\Phi = D\Phi_2 \circ D\Phi_1$  (30). Here  $\Phi_2 = (\pi \times \pi)^{\times 5}$  whence  $D\Phi_2 = (D\pi \oplus D\pi)^{\oplus 5}$  and  $\ker(D\Phi_2)((\Gamma_1, \bar{\Gamma}_1), \dots, (\Gamma_5, \bar{\Gamma}_5)) = \mathbb{R}\Gamma_1 \oplus \dots \oplus \mathbb{R}\bar{\Gamma}_5$ . Also  $D\Phi_1$  takes the explicit form determined in Proposition 16. In the appendices, we argue that (34) can be reduced to the  $5 \times 5$  linear system:

$$\begin{aligned} a((\Gamma_i)_1^2 + (\Gamma_i)_2^2) + b(\Gamma_i)_1(\Gamma_i)_3 + c(\Gamma_i)_2(\Gamma_i)_3 \\ + d(\Gamma_i)_2 + e(\Gamma_i)_2 = 0 \end{aligned}$$

for  $i = 1, \dots, 5$ . It has a nonzero solution if and only if there exists  $\mathcal{Q}$  passing through  $\Gamma_1, \dots, \Gamma_5$ , as announced.  $\square$

See Fig. 2 for visualizations of Theorem 18. Note that the second bullet in Theorem 18 implies  $\mathcal{Q}$  is ruled, *i.e.* covered by lines. The third bullet implies that  $\mathcal{Q}$  is a “rectangular quadric” as defined in [36, Ch. 3.2].

**Theorem 19.** Consider the 7-point problem from Section 2.2.

Let  $w = (b, \Gamma_1, \dots, \Gamma_7) \in \mathcal{W}$ , written as in Lemma 4. Then  $w \in \text{ill}(\mathcal{M}, \mathcal{W})$  if and only if there exists a quadric surface  $\mathcal{Q}$  in  $\mathbb{R}^3$  such that:

- $\Gamma_i \in \mathcal{Q}$  for each  $i = 1, \dots, 7$ ;

- $\ell \subseteq \mathcal{Q}$  where  $\ell$  is the baseline through the two camera centers.

**Sketch:** Let  $\delta w = (\delta b, \delta \Gamma_1, \dots, \delta \Gamma_7) \in T(\mathcal{W}, w)$ . Again we wish to characterize when

$$D\Phi(w)(\delta w) = 0 \quad (35)$$

has a nonzero solution in  $\delta w$ . We use  $D\Phi = D\Phi_2 \circ D\Phi_1$ , where  $D\Phi_2 = (D\pi \oplus D\pi)^{\oplus 7}$  and  $D\Phi_1$  is as in the proof of Proposition 17. Eliminating variables, we reduce (35) to a particular  $7 \times 7$  linear system. Its solvability is equivalent to there existing a quadric surface  $\mathcal{Q}$  as described. See details in the appendices.  $\square$

### 4.3 Ill-posed image data

We describe ill-posed image data for the 5- and 7-point problems.

**Theorem 20.** Consider the 5-point problem from Section 2.1.

Let  $x = ((\gamma_1, \bar{\gamma}_1), \dots, (\gamma_5, \bar{\gamma}_5)) \in (\mathbb{R}^2 \times \mathbb{R}^2)^{\times 5}$  be image data. Then  $x \in \text{ill}(\mathcal{M}, \mathcal{X})$  only if a certain polynomial  $\mathbf{P}$  in the entries of  $\gamma_1, \dots, \bar{\gamma}_5$  vanishes. Further,  $\mathbf{P}$  has degree 30 separately in each of  $\gamma_1, \dots, \bar{\gamma}_5$ .

**Remark 21.** An explicit form for  $\mathbf{P}$  is currently not available. Nonetheless, we can still compute with specializations of  $\mathbf{P}$ . Specifically, suppose we fix  $\gamma_1, \bar{\gamma}_1, \dots, \gamma_5$  but keep  $\bar{\gamma}_5 \in \mathbb{R}^2$  as a variable. Then generically,  $\mathbf{P}$  is a degree-30 polynomial in just  $\bar{\gamma}_5$ . Its zero set is a plane curve. We show how to plot such curves in Section 6.

**Sketch:** As noted in Example 11, the 5-point problem has an epipolar map  $\mathbf{L}$  in the sense of Definition 10 with  $n = 8$  and  $d = 5$ . Therefore Theorem 13 applies. It implies the existence of a nonzero polynomial  $\mathbf{P}$  in the Plücker coordinates for codimension-5 linear subspaces of  $\mathbb{P}_{\mathbb{R}}^8$  such that (25) holds. Here  $\mathcal{Y}_{\mathbb{C}} = \{E \in \mathbb{P}(\mathbb{C}^{3 \times 3}) : 2EE^T E - \text{tr}(EE^T)E = 0, \det(E) = 0\}$ . By [46, Ex. 2.5], this variety has degree  $p = 10$  and sectional genus  $g = 6$ . By [22, Prop. 2], the singular locus of  $\mathcal{Y}_{\mathbb{C}}$  has codimension 3. So, Theorem 13 implies the degree of  $\mathbf{P}$  is  $2 \cdot 10 + 2 \cdot 6 - 2 = 30$  in Plücker coordinates. From the constraints in Example 11, each maximal minor of  $\mathbf{L}(x)$  is multi-affine in  $\gamma_1, \dots, \bar{\gamma}_5$ . So,  $\mathbf{P}$  has degree 30 separately in each of  $\gamma_1, \dots, \bar{\gamma}_5$ .

To conclude, use Proposition 15. It suffices to verify the property there, which states that given image data  $x$  outside of the discriminant, a compatible world scene and essential matrix, we can smoothly locally lift the essential matrix and  $x$  to the world scene as  $x$  moves. This is justified in the appendices using [26, Result 9.19] and [49].  $\square$

A similar characterization holds in the uncalibrated case, except it is more explicit.

**Theorem 22.** Consider the 7-point problem from Section 2.2.

Let  $x = ((\gamma_1, \bar{\gamma}_1), \dots, (\gamma_7, \bar{\gamma}_7)) \in (\mathbb{R}^2 \times \mathbb{R}^2)^{\times 7}$  be image data. Then  $x \in \text{ill}(\mathcal{M}, \mathcal{X})$  only if a certain polynomial  $\mathbf{P}$  in the entries of  $\gamma_1, \dots, \bar{\gamma}_7$  vanishes. The polynomial has degree 6 separately in each of  $\gamma_1, \dots, \bar{\gamma}_7$ . In fact,  $\mathbf{P}$  can be expressed as an explicit degree-6 polynomial in the 36 Plücker coordinates for 2-dimensional subspaces of  $\mathbb{R}^9$ , with 1668 monomial terms and all coefficients integers at most 72 in absolute value.

**Remark 23.** Suppose we fix  $\gamma_1, \bar{\gamma}_1, \dots, \gamma_7$ , but keep  $\bar{\gamma}_7$  as a variable. Then generically,  $\mathbf{P}$  is a degree-6 polynomial in just  $\bar{\gamma}_7$ . Its zero set is a plane curve. In Section 6 we compute these curves to visualize  $\text{ill}(\mathcal{M}, \mathcal{X})$ .

**Sketch:** The 7-point problem has an epipolar map, with  $n = 8$  and  $d = 7$ . By Theorem 13, there is a nonzero polynomial  $\mathbf{P}$  in the  $\binom{9}{7} = 36$  Plücker coordinates for lines in  $\mathbb{P}_{\mathbb{R}}^8$  that obeys (25). Here  $\mathcal{Y}_{\mathbb{C}} = \{F \in \mathbb{P}(\mathbb{C}^{3 \times 3}) : \det(F) = 0\}$  has degree  $p = 3$  and sectional genus  $g = 1$ . So  $\mathbf{P}$  has degree  $2 \cdot 3 + 2 \cdot 1 - 2 = 6$  in Plücker coordinates. As in Theorem 20, this implies that  $\mathbf{P}$  has degree 6 separately in each of  $\gamma_1, \dots, \bar{\gamma}_7$  as wanted. In Section 6 we compute  $\mathbf{P}$  explicitly, using the formula for the discriminant of a univariate cubic polynomial. In the appendices we verify the smooth lifting property using [26, Result 9.14].  $\square$

## 5 RELATION BETWEEN ILL-POSEDNESS, DEGENERACY AND CRITICALITY

In this section we compare our notions to thoroughly-studied ones in the literature.

Previous works in multiview geometry have considered degenerate image data and critical world scenes, e.g. [8], [26], [28], [29], [32], [36]. Criticality and degeneracy fundamentally concern *uniqueness*. They are defined as follows.

**Definition 24.** (e.g. [48, Sec. 2.1]) Consider a (not necessarily minimal) multiview geometry estimation problem. A configuration of noiseless image data is called **degenerate** if the corresponding epipolar geometry is not unique.

**Definition 25.** (e.g. [29]) Consider a (not necessarily minimal) multiview geometry estimation problem. A world scene is called **critical** if it maps to degenerate image data.

Studying these concepts, other researchers have classified scenarios when there are multiple solutions to the 3D reconstruction problems. This line of work is primarily about the super-minimal case. For example, it answers questions of the following sort: For which scenes of two uncalibrated cameras and 50 world points does there exist an inequivalent world scene mapping to the same image data? In particular, degeneracy and criticality seem unhelpful for minimal problems: those usually have multiple solutions.

The concepts of ill-posed world scenes and image data in Definitions 8 and 9 are different. They pertain to minimal problems. Furthermore, instead of uniqueness, ill-posedness captures when one (of possibly multiple) solutions is unstable. More precisely, the condition number is infinite.

That said, in two-view geometry critical world scenes have been characterized in terms of quadric surfaces too, see [32] and [28]. In the uncalibrated case, there is a critical ruled quadric in the literature, like ours in Theorem 19, except it is only required to contain the world points and camera centers and not the baseline. The calibrated case is analogous, with “ruled quadric” replaced by “rectangular quadric”. Our next result serves to clarify the relationship.

**Proposition 26.** Consider a super-minimal world scene  $w'$ , consisting of two calibrated cameras and  $N$  world points where  $N \geq 5$ . Assume that for each subset of 5 world points, the resulting minimal world scene  $w$  is ill-posed.

Then  $w'$  is critical. The same statement holds with “calibrated” and “5” replaced by “uncalibrated” and “7”.

**Sketch:** For each minimal subscene  $w$ , there exists a quadric surface satisfying the conditions in Theorem 18. In the appendices, we view the conditions as linear in the quadric and prove that there must exist a common quadric  $\mathcal{Q}$  which works for each  $w$ . In particular,  $\mathcal{Q}$  passes through the two camera centers and  $N$  world points of  $w'$ . So  $w'$  is critical by [28]. The uncalibrated case is the same.  $\square$

The proposition is tight: if there exists *one* minimal subscene  $w$  that is well-posed, then  $w'$  can be nondegenerate. We also stress that the converse of Proposition 26 fails. Indeed if  $w'$  is critical, then *all* minimal subscenes  $w$  could be well-posed, as illustrated below.

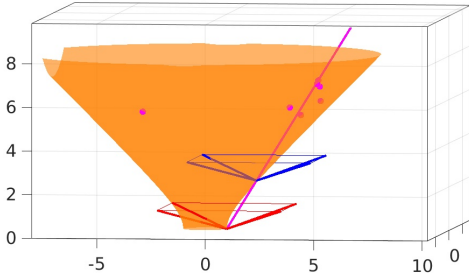


Fig. 3. Example of an uncalibrated scene that is critical, in which all minimal subscenes are well-posed. Fix a ruled quadric surface (orange surface) as shown. Any  $N$  points and 2 camera centers (magenta points) drawn from the quadric will form a critical configuration by [32]. However generically, the baseline (magenta line) will not lie on the surface.

## 6 COMPUTATION OF X.5-POINT CURVES

We explain how to compute the curves in Remarks 21 and 23, dubbed “4.5-point” and “6.5-point” curves for short. The curves represent the ill-posed loci in image data space.

### 6.1 Numerical computation of X.5-point curves

There is a numerical method to render the X.5-point curves in both the calibrated and uncalibrated cases. It is based on homotopy continuation [9]. We describe the procedure only for the calibrated case, as the uncalibrated case is analogous.

To generate the 4.5-point curve, four image point pairs  $(\gamma_i, \bar{\gamma}_i)$  for  $i = 1, \dots, 4$  and a stand-alone point  $\gamma_5$  are fixed. Using SVD, we compute the null space of the linear system  $(\bar{\gamma}_i; 1)^\top E(\gamma_i; 1) = 0$  for  $i = 1, \dots, 4$ . If it is more than 5-dimensional as in [16], then all choices of  $\bar{\gamma}_5$  give a point in the ill-posed locus. Otherwise, similarly to [38] we parameterize (an affine slice of) the null space as

$$E = E(\alpha) := \alpha_1 E_1 + \alpha_2 E_2 + \alpha_3 E_3 + \alpha_4 E_4 + E_5, \quad (36)$$

where  $E_i$  are a basis of the null space and  $\alpha_i$  are unknown weights. The essential matrix should also satisfy

$$\begin{cases} \det(E) = 0 \\ 2EE^\top E - \text{tr}(EE^\top)E = 0, \end{cases} \quad (37)$$

which are 10 cubic equations. Further, the fifth correspondence should satisfy the epipolar constraint

$$(\bar{\gamma}_5; 1)^\top E(\gamma_5; 1) = 0. \quad (38)$$

At ill-posed configurations, the Jacobian matrix of the constraints (37) and (38) with respect to  $\alpha_i$  should be rank-deficient. The Jacobian  $J$  is a  $11 \times 4$  matrix. To enforce its rank-deficiency, we introduce 3 dummy variables  $d_1, d_2, d_3 \in \mathbb{R}$  and require

$$J(d_1 \ d_2 \ d_3 \ 1)^\top = 0. \quad (39)$$

Note that there are 22 equations from (37), (38), (39) and altogether 9 unknowns, namely  $\alpha_1, \alpha_2, \alpha_3, \alpha_4, (\bar{\gamma}_5)_1, (\bar{\gamma}_5)_2, d_1, d_2, d_3$ . The solutions to this polynomial system, projected to the  $\bar{\gamma}_5$ -plane, define the 4.5-point curve.

By setting  $(\bar{\gamma}_5)_1$  to various different values, we compute the zero-dimensional solution sets as in Fig. 4. The real solutions for  $(\bar{\gamma}_5)_2$  correspond to the intersection between the 4.5-point curve and a column of the image. The solutions to these systems are computed using parameter homotopy [9]. By Theorem 20, the systems have 30 complex solutions, so there are at most 30 real intersections with the various columns of the second image. Linearly connecting the intersection points, the 4.5-point curve is rendered. Based on our experiments, computing the intersection points for each choice of  $(\bar{\gamma}_5)_1$  takes about 10 ms on a desktop computer.

In applications we may wish to estimate the condition number by approximating (22) as the reciprocal distance from a target point to the curve. Then a full plot of the curve is not required. We can simply compute the intersection points as  $(\bar{\gamma}_5)_1$  ranges over a small interval around the correspondence candidate, see Fig. 4(b).

Finally, computations for different columns of the image are independent. So the procedure is easily parallelized.

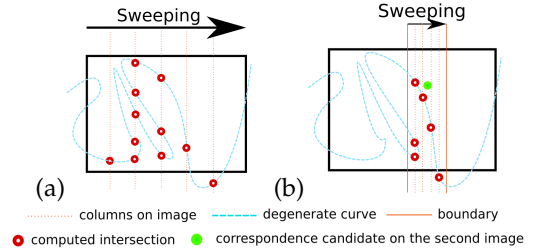


Fig. 4. (a) To generate X.5-point curves on the second image, we can sweep the image columnwise and compute the intersection with vertical lines by solving (37), (38), (39). (b) To assess a candidate correspondence, we can scan just a neighborhood around the candidate point.

### 6.2 Symbolic computation of 6.5-point curves

The numerical method in Section 6.1 can generate the 4.5-point and 6.5-point curves with high precision. However, given the iterative nature of homotopy continuation, it is slow in finding the distance from the point to the curve. Engineering with GPUs has accelerated homotopy continuation path-tracking methods as much as  $100\times$  (see [13], [14], [50]), but the speedup factor varies across problems. Alternatively, for the case of 6.5-point curves, we can symbolically compute the defining equation of the curve with high speed. This is based on the last sentence of Theorem 22.

First, we derive the expression for  $\mathbf{P}$  in Theorem 22. Consider the  $7 \times 9$  matrix encoding the epipolar constraints:

$$\mathbf{L}((\gamma_1, \bar{\gamma}_1), \dots, (\gamma_7, \bar{\gamma}_7)) \quad (40)$$

from Example 11. Let its maximal minors be  $p_{ij}$  for  $1 \leq i < j \leq 9$ , obtained by dropping the  $i$ th and  $j$ th columns. If these are all 0, then (40) is rank-deficient and  $\mathbf{P}$  vanishes. Else,  $p_{ij}$  are the Plücker coordinates for the row-span of (40). Each  $p_{ij}$  is a degree-6 polynomial in 14 symbolic variables. Generically, a basis for the null space of (22) is written as

$$F_1 = \begin{pmatrix} 0 & 1 & p_{13} \\ p_{14} & p_{15} & p_{16} \\ p_{17} & p_{18} & p_{19} \end{pmatrix}, F_2 = \begin{pmatrix} 1 & 0 & -p_{23} \\ -p_{24} & -p_{25} & -p_{26} \\ -p_{27} & -p_{28} & -p_{29} \end{pmatrix}. \quad (41)$$

Let  $F = F(t) = tF_1 + F_2$ , where  $t$  is an unknown weight. The fundamental matrix must satisfy the constraint

$$\det(F) = 0. \quad (42)$$

At ill-posed image data, (42) should have a double root with respect to  $t$ . So the discriminant of (42) (a univariate cubic) vanishes. Substituting (41) into the discriminant in [24] produces the wanted expression for  $\mathbf{P}$  in terms of  $p_{ij}$ .

As for the 6.5-point curve, plug numerical values for  $\gamma_1, \bar{\gamma}_1, \dots, \gamma_7$  into (40). Taking maximal minors, compute the Plücker coordinates  $p_{ij}$  as affine-linear polynomials in  $(\bar{\gamma}_7)_1, (\bar{\gamma}_7)_2$ . Substitute these into the expression for  $\mathbf{P}$  to get the defining equation for the curve. With the defining equation in hand, we estimate the distance to a target point by the Sampson distance approximation [26]. We optimize this procedure using Maple to minimize the number of arithmetical operations needed to compute the 6.5-point curve in C++. In experiments below, we achieve an average speed of  $200\mu\text{s}$  per 6.5-point curve on a single CPU, which reaches real-time speeds. The computation could be further sped-up, by calculating different coefficients in parallel.

## 7 EXPERIMENTAL RESULTS

This section presents numerical experiments. Corresponding code may be found at: <https://github.com/HongyiFan/minimalInstability>.

### 7.1 Instability with only inliers present

We first aim to demonstrate that instabilities do occur in practice for relative pose estimation problems. We show epipolar estimation can fail even with no outliers in the data.

To this end, we generate 3000 random instances of the 5- and 7-point minimal problems. First, generate random world scenes  $(\mathbf{R}, \hat{\mathbf{T}}, \Gamma_1, \dots, \Gamma_N)$  with  $N = 7$  and an intrinsic matrix  $K$  in the uncalibrated case, and otherwise with  $N = 5$  in the calibrated case, as follows:

- $\mathbf{R}$ : taken from the QR decomposition of a random  $3 \times 3$  matrix with i.i.d. standard normal entries;
- $\hat{\mathbf{T}}$ : a uniformly-sampled point on the sphere with radius 1 meter;
- $\Gamma_i$ : uniformly-sampled world points with depths between 1 and 20 meters;
- $K$ : chosen so the image size is  $640 \times 480$ , focal length is 32 mm and principle point is the image center.

Then we compute clean image data  $(\gamma_i, \bar{\gamma}_i)$  for  $i = 1, \dots, N$  as the projections of  $\Gamma_i$  onto the two images. We discard and regenerate an instance if any of the 2D points fall outside of

the image’s boundary, or if any of the 3D points are located at the behind the cameras. Finally, i.i.d. noise is added to each image point, drawn from the 2D Gaussian distribution  $\mathcal{N}(0, \sigma^2 I)$ , for different noise levels  $\sigma$ .

Next, we separately solve the clean and perturbed minimal problems using the standard solvers. Here we regard an instance as unstable if either: (i) there is a large error in the computed epipolar matrix for the perturbed data; or (ii) there is a difference in the number of real solutions for the clean and perturbed data. In criterion (i), the error in the fundamental or essential matrix is taken as  $e = \text{mean}(\text{abs}(\text{abs}(\bar{M}/M) - \mathbf{1}\mathbf{1}^\top))$  where “./” denotes elementwise division, “abs” denotes entrywise absolute value,  $\mathbf{1}$  is the all-ones vector,  $M$  is the ground-truth model and  $\bar{M}$  is the nearest estimated real model. If  $e \geq \tau$  for some threshold  $\tau$ , then the instance is counted as unstable. Meanwhile, criterion (ii) is included because the number of real solutions changes only if the ill-posed locus is crossed [5].

Fig. 5 shows the fraction of unstable instances out of the 3000 runs, at small to moderate noise levels and various error thresholds. We stress that all image point pairs are inliers here. Even so, it is clear that for random perturbations the occurrence of unstable cases cannot be ignored.

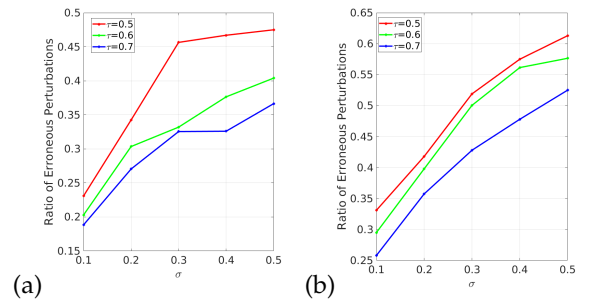


Fig. 5. Ratio of unstable instances out of 3000 random synthetic minimal problem instances at different noise levels  $\sigma$  and error thresholds  $\tau$  for: (a) fundamental matrices; and (b) essential matrices.

Given that minimal problems have such failure rates, many point pairs are needed for RANSAC to overcome these instabilities. We test this by generating calibrated world scenes as before, but with the number  $N$  of world points much more than 5. Add i.i.d. Gaussian noise, with  $\sigma$  drawn uniformly from  $[0, 2]$  pixels in each trial. The datasets again have no outliers. We apply a standard RANSAC method to estimate the essential matrix. Fig. 6 shows results over 100 trials for two different choices of  $N$ . With  $N = 50$ , the median rotation and translation errors are  $> 10^\circ$  and  $> 1$  pixels respectively. The errors improve when  $N = 150$ .

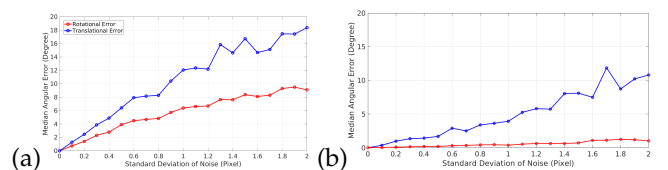


Fig. 6. Median translation error and rotation error (both in degrees) vs. standard deviation of noise (in pixels) over 100 synthetic scenes for: (a)  $N = 50$  veridical correspondences; and (b)  $N = 150$  veridical correspondences. More point pairs lead to less error in RANSAC.

## 7.2 Instability estimation by X.5-point curves

We apply the methods in Section 6 to render the 4.5- and 6.5-point curves. Fig. 7 shows several example curves plotted on the second image plane along with the given image points. For the uncalibrated case the degree of the curve is 6 by Theorem 22, while for calibrated case it is 30 by Theorem 20.

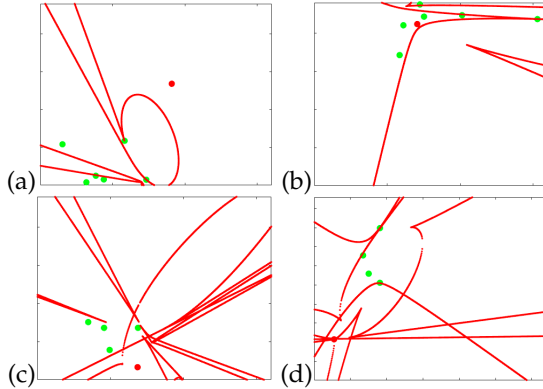


Fig. 7. Example renderings of X.5-point curves. The condition number is approximately the reciprocal distance from the red point to the curve. (a) Well-conditioned configuration for  $F$  estimation. (b) Poorly-conditioned configuration for  $F$  estimation. (c) Well-conditioned configuration for  $E$  estimation. (d) Poorly-conditioned configuration for  $E$  estimation.

In another test, we sort the 3000 random synthetic minimal problems from Section 7.1 into three categories: stable, unstable, and borderline cases. Here, an instance is classified according to the number of erroneous estimates among  $n = 20$  perturbations, denoted by  $\hat{n}$ . If  $\hat{n} \in [0, n/3]$  we count the instance as stable; if  $\hat{n} \in [2n/3, n]$  we count it as unstable; while if  $\hat{n} \in [n/3, 2n/3]$  we count it as borderline. We take  $\tau = 0.5$  and  $\sigma = 0.3$ . In the uncalibrated case, the average distance from the 7th point to the 6.5-point curve is 2.35 pixels among unstable cases, while for the stable cases it is 22.12 pixels. In the calibrated case, the average distance from the 5th point to the 4.5-point curve is 0.32 pixels for unstable cases, while for the stable case it is 14.95 pixels. See the histograms in Fig. 8. Given the statistical differences, the stable and unstable categories are distinguished by the distance from the last point to the X.5-point curve.

We next check the relationship between the condition number, the pose estimation error and the distance from the target point to X.5-point curve. Results over the 3000 scenes are plotted in Fig. 9. As expected, there is a linear relationship between the maximum error in rotation/translation and the computed condition number (Fig. 9(a)). We also see an inverse-linear relationship between the distance from the point to the X.5-point curve and the maximum error in the rotation/translation (Fig. 9(b)), as expected.

Last, we show that the X.5-point curves themselves are acceptably stable to perturbations in the image data. Fig. 10 displays examples of the X.5-point curves when adding noise to the image points. Note that the curves do not drastically change. Fig. 11 collects the statistics over the 6000 different minimal problems (half calibrated and half uncalibrated), when the perturbations are Gaussian with a standard deviation of 1 pixel. We find that the distance to the X.5-point curve is sufficiently robust to be used in practice.

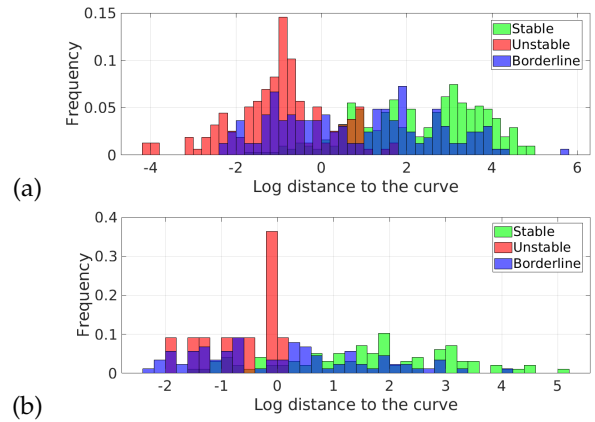


Fig. 8. Histograms of distance from the last point to the X.5-point curve sorted by: stable cases (green), unstable cases (red) and borderline cases (blue). (a) Uncalibrated estimation. (b) Calibrated estimation. Stable and unstable categories are separated by distance to the curve.

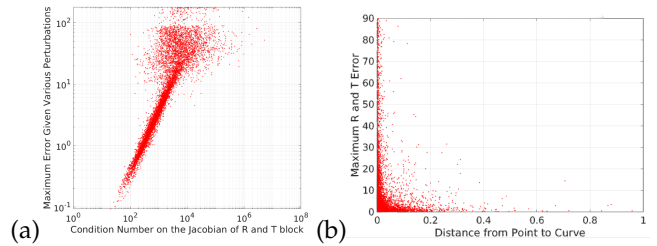


Fig. 9. Comparison of the condition number, pose estimation error, and distance from the target point to the X.5-point curve. (a) Linear relationship between the maximum rotation/translation error among various perturbations on the image point pairs vs. the condition number computed using Proposition 17. As expected, the linear relation breaks down when the noise is high. (b) Inverse-linear relationship between the maximum rotation/translation error among various perturbation on the image point pairs vs. the distance from the point to 6.5-point curve.

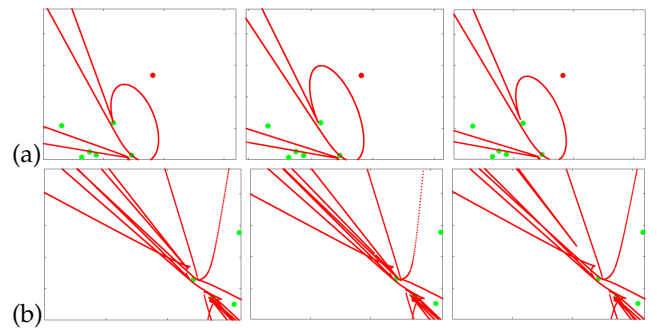


Fig. 10. Illustration of the stability of the X.5-point curves themselves. (a) A 6.5-point curve for uncalibrated estimation with different perturbations on the image points applied. (b) A 4.5-point curve for calibrated estimation with different perturbations on the image points applied.

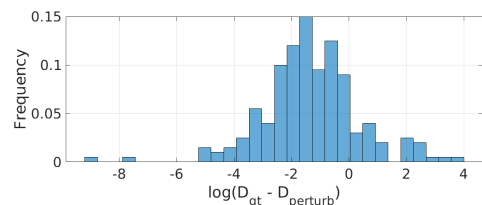


Fig. 11. Histogram of the log-difference between two distances: from the target point to the X.5-point curve without perturbation; and from the target point to the X.5-point curve with perturbation on the other points.

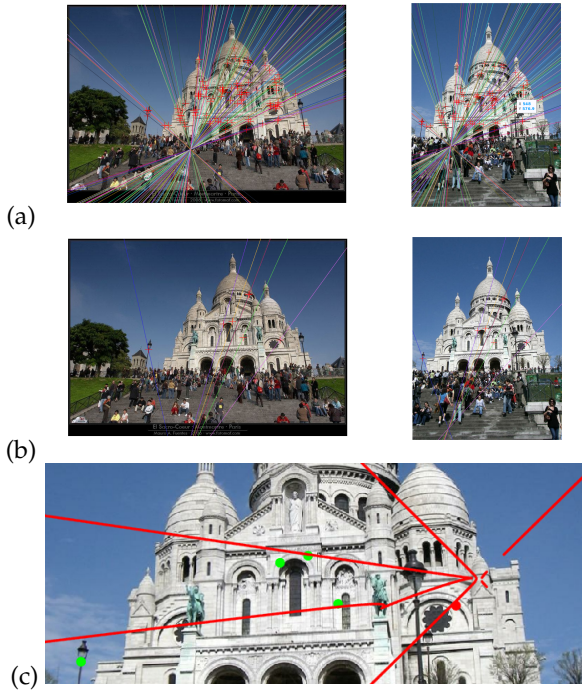


Fig. 12. Example with real data demonstrating an unstable minimal configuration from all-inlier correspondences. (a) The ground-truth epipolar geometry of a pair of images. (b) The closest solution found by the 7-point algorithm give seven inliers. (c) Zoomed-in image showing that the remaining point is close to the 6.5-point curve. This indicates the minimal instance is poorly conditioned, so the errors in (b) are expected.

### 7.3 Illustrations with real data

We first demonstrate that the failure of RANSAC described at the end of Section 7.1 can occur with real data. To this end, we take various overlapping pairs of images from the RANSAC 2020 dataset [37], manually remove all outliers, and then apply a standard RANSAC procedure to estimate the epipolar geometries. Despite there being all inliers, this estimation suffers errors of  $> 10^\circ$  in the rotation for  $> 50\%$  of image pairs, similarly to the synthetic experiments in Section 7.1. A sample result with real data is shown in Fig. 1.

Next, we illustrate utility of the X.5-point curve on real data. Again we use image pairs from the RANSAC 2020 dataset [37], where veridical image point correspondences are available. Fig. 12 shows that for a minimal instance in which standard minimal solvers have large errors, the selected image point indeed lies close to the X.5-point curve. It is consistent with our theory, because such data instances are poorly-conditioned.

Last, we note that X.5-point curves might also be useful in near-degenerate situations (recall the comparison made in Section 5). For example, consider near-planar scenes. It is well-known that the near-planar scenes are nearly degenerate. However, their minimal subscenes are also ill-posed by Theorems 18 and 19. In the uncalibrated case, for example, minimal subscenes with at least two off-plane points would be both stable as well as non-degenerate. If the distance from a selected point to the 6.5-point curve is large, it could help in identifying good minimal instances. The idea is illustrated in Fig. 13.

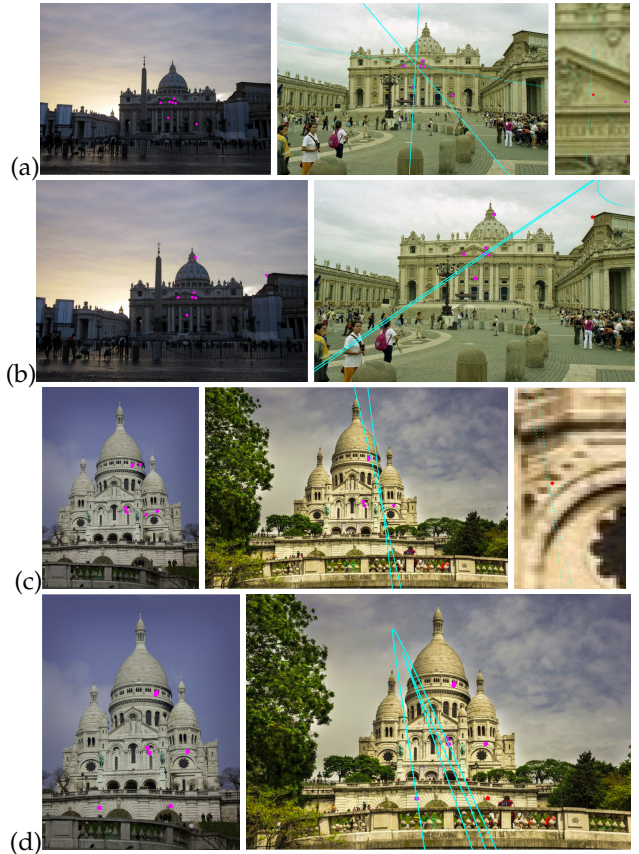


Fig. 13. Illustrative results showing how the 6.5-point curve may help with near-planar world scenes. (a)(c) 7 near-planar point pair selections (magenta) generate small distances from the target point (red) to the 6.5-point curve (cyan). (b)(d) 5 near-planar point pair selections and 2 off-plane point pairs (magenta) generate large distance from the target point (red) to the 6.5-point curve (cyan).

## 8 CONCLUSION

Stability has been largely ignored in multiview geometry. To the extent it has been considered, it has been conflated with degeneracy and criticality. In this paper, we presented a general framework for analyzing instabilities of minimal problems. We defined condition numbers as well as ill-posed world scenes and image data. General methods were introduced and used to analyze the 5- and 7-point problems in relative pose estimation. Numerical experiments on synthetic and real data support our theory, and suggest that instabilities negatively impact RANSAC in practice.

The opportunities for future work are numerous. To name a few, first we would like to apply the framework to analyze other important minimal problems in multiview geometry. Second, it is very desirable to make RANSAC “stability-aware”, e.g. by biasing its sampling towards well-conditioned image data, perhaps by building on [3]. Third, we propose using related theory [10] to analyze the conditioning of bundle adjustment.

## REFERENCES

[1] D. Ablan. *Digital Photography for 3D Imaging and Animation*. Wiley, 2007. 1  
 [2] S. Agarwal, Y. Furukawa, N. Snavely, I. Simon, B. Curless, S. M. Seitz, and R. Szeliski. Building Rome in a day. *Communications of the ACM*, 54(10):105–112, 2011. 1

- [3] D. Barath, L. Cavalli, and M. Pollefeys. Learning to find good models in ransac. In *CVPR*, pages 15744–15753, 2022. **11**
- [4] D. Barath, J. Noskova, M. Ivashechkin, and J. Matas. MAGSAC++, a fast, reliable and accurate robust estimator. In *CVPR*, pages 1304–1312, 2020. **1**
- [5] E. A. Bernal, J. D. Hauenstein, D. Mehta, M. H. Regan, and T. Tang. Machine learning the real discriminant locus. *Journal of Symbolic Computation*, 115:409–426, 2023. **9**
- [6] N. Bourbaki. *General Topology: Chapters 1–4*, volume 18. Springer, 2013. **12**
- [7] E. Brachmann and C. Rother. Neural-guided RANSAC: Learning where to sample model hypotheses. In *CVPR*, pages 4322–4331, 2019. **1**
- [8] M. Bråtelund. Critical configurations for two projective views, a new approach. *Journal of Symbolic Computation*, 120:102226, 2024. **2, 7**
- [9] P. Breiding and S. Timme. HomotopyContinuation.jl: A package for homotopy continuation in Julia. In *Mathematical Software–ICMS 2018: 6th International Conference, South Bend, IN, USA, July 24–27, 2018, Proceedings 6*, pages 458–465. Springer, 2018. **8**
- [10] P. Breiding and N. Vannieuwenhoven. The condition number of Riemannian approximation problems. *SIAM Journal on Optimization*, 31(1):1049–1077, 2021. **11**
- [11] P. Burgisser. Condition of intersecting a projective variety with a varying linear subspace. *SIAM Journal on Applied Algebra and Geometry*, 1(1):111–125, 2017. **5**
- [12] P. Bürgisser and F. Cucker. *Condition: The Geometry of Numerical Algorithms*, volume 349. Springer, 2013. **4**
- [13] C.-H. Chien, H. Fan, A. Abdelfattah, E. Tsigaridas, S. Tomov, and B. Kimia. GPU-based homotopy continuation for minimal problems in computer vision. In *CVPR*, pages 15765–15776, 2022. **8**
- [14] C.-H. Chien, H. Fan, A. Abdelfattah, E. Tsigaridas, S. Tomov, and B. Kimia. Parallel path tracking for homotopy continuation using GPU. In *Proceedings of the International Symposium on Symbolic and Algebraic Computation*, 2022. **8**
- [15] O. Chum, J. Matas, and J. Kittler. Locally optimized RANSAC. In *Joint Pattern Recognition Symposium*, pages 236–243. Springer, 2003. **1**
- [16] E. Connelly, S. Agarwal, A. Ergur, and R. R. Thomas. The geometry of rank drop in a class of face-splitting matrix products. *arXiv preprint arXiv:2301.09826*, 2023. **8**
- [17] M. Demazure. *Sur Deux Problèmes De Reconstruction*. PhD thesis, INRIA, 1988. **3**
- [18] J. W. Demmel. On condition numbers and the distance to the nearest ill-posed problem. *Numerische Mathematik*, 51(3):251–289, 1987. **5**
- [19] T. Dobbert. *Matchmoving: The Invisible Art of Camera Tracking*. Sybex, 2005. **1**
- [20] T. Duff, K. Kohn, A. Leykin, and T. Pajdla. PL1P-Point-Line minimal problems under partial visibility in three views. In *ECCV*, pages 175–192, 2020. **4**
- [21] H. Fan, J. Kileel, and B. Kimia. On the instability of relative pose estimation and RANSAC’s role. In *CVPR*, pages 8935–8943, 2022. **2**
- [22] G. Fløystad, J. Kileel, and G. Ottaviani. The Chow form of the essential variety in computer vision. *Journal of Symbolic Computation*, 86:97–119, 2018. **7**
- [23] G. H. Golub and C. F. Van Loan. *Matrix Computations*. JHU press, 2013. **4**
- [24] D. R. Grayson and M. E. Stillman. Macaulay2, a software system for research in algebraic geometry. <http://www.math.uiuc.edu/Macaulay2/>. **9**
- [25] J. Harris. *Algebraic Geometry: A First Course*, volume 133. Springer, 2013. **4**
- [26] R. Hartley and A. Zisserman. *Multiple View Geometry in Computer Vision*. CUP, 2nd edition, 2004. **1, 2, 3, 4, 7, 9, 13, 17**
- [27] B. Horn. *Robot Vision*. MIT press, 1986. **1**
- [28] F. Kahl and R. Hartley. Critical curves and surfaces for Euclidean reconstruction. In *ECCV*, pages 447–462, 2002. **2, 7, 8**
- [29] F. Kahl, R. Hartley, and K. Åström. Critical configurations for  $n$ -view projective reconstruction. In *CVPR*, volume 2, 2001. **2, 7**
- [30] Y. Kasten, A. Geifman, M. Galun, and R. Basri. Algebraic characterization of essential matrices and their averaging in multiview settings. In *CVPR*, pages 5895–5903, 2019. **1**
- [31] M. Kitagawa and B. Windsor. *MoCap for Artists: Workflow and Techniques for Motion Capture*. Focal Press, 2008. **1**
- [32] J. Krames. Zur ermittlung eines objektes aus zwei perspektiven (ein beitrag zur theorie der “gefährlichen örter”). *Monatshefte für Mathematik und Physik*, 49(1):327–354, 1941. **2, 7, 8**
- [33] J. M. Lee. *Riemannian Manifolds: An Introduction to Curvature*, volume 176. Springer, 2006. **18**
- [34] J. M. Lee. *Smooth Manifolds*. Springer, 2013. **2, 3, 4, 5, 13, 14**
- [35] T. Luhmann, S. Robson, S. Kyle, and I. Harley. *Close Range Photogrammetry: Principles, Methods, and Applications*. Wiley, 2007. **1**
- [36] S. Maybank. *Theory of Reconstruction From Image Motion*, volume 28. Springer, 2012. **2, 6, 7**
- [37] D. Mishkin. Benchmarking robust estimation methods. CVPR Tutorial: RANSAC in 2020. <https://github.com/ducha-aiki/ransac-tutorial-2020-data>. **1, 11**
- [38] D. Nistér. An efficient solution to the five-point relative pose problem. *IEEE Transactions on Pattern Analysis and Machine Intelligence*, 26(6):756–770, 2004. **1, 3, 8**
- [39] O. Özyeşil, V. Voroninski, R. Basri, and A. Singer. A survey of structure from motion. *Acta Numerica*, 26:305–364, 2017. **1**
- [40] R. Penrose. A generalized inverse for matrices. In *Mathematical Proceedings of the Cambridge Philosophical Society*, volume 51, pages 406–413. CUP, 1955. **13, 14**
- [41] M. Pollefeys, L. Van Gool, M. Vergauwen, K. Cornelis, F. Verbiest, and J. Tops. Image-based 3D acquisition of archaeological heritage and applications. In *Conference on Virtual Reality, Archaeology, and Cultural Heritage*, pages 255–262, 2001. **1**
- [42] R. Raguram, J.-M. Frahm, and M. Pollefeys. A comparative analysis of RANSAC techniques leading to adaptive real-time random sample consensus. In *ECCV*, pages 500–513, 2008. **1**
- [43] J. L. Schönberger and J.-M. Frahm. Structure-from-motion revisited. In *CVPR*, pages 4104–4113, 2016. **1**
- [44] S. M. Seitz, B. Curless, J. Diebel, D. Scharstein, and R. Szeliski. A comparison and evaluation of multi-view stereo reconstruction algorithms. In *CVPR*, pages 519–528, 2006. **1**
- [45] C. V. Stewart. Robust parameter estimation in computer vision. *SIAM Review*, 41(3):513–537, 1999. **1**
- [46] B. Sturmfels. The Hurwitz form of a projective variety. *Journal of Symbolic Computation*, 79:186–196, 2017. **5, 7**
- [47] R. Szeliski. *Computer Vision: Algorithms and Applications*. Springer, 2010. **1**
- [48] P. H. Torr, A. Zisserman, and S. J. Maybank. Robust detection of degenerate configurations while estimating the fundamental matrix. *Computer Vision and Image Understanding*, 71(3):312–333, 1998. **7**
- [49] R. Tron and K. Daniilidis. The space of essential matrices as a Riemannian quotient manifold. *SIAM Journal on Imaging Sciences*, 10(3):1416–1445, 2017. **7, 17**
- [50] J. Verschelde and X. Yu. Polynomial homotopy continuation on GPUs. *ACM Communications in Computer Algebra*, 49(4):130–133, 2016. **8**

## APPENDIX A PROOF OF PROPOSITION M-1

Let  $\mathcal{V}$  denote the open subset of  $\mathcal{C}^{\times 2} \times (\mathbb{R}^3)^{\times 5}$  in (M-1).

The action (M-2) is clearly smooth.

For freeness, we must show that each stabilizer is trivial. Equivalently, each orbit contains a point with trivial stabilizer. Note that each orbit contains a point  $v = (P, \bar{P}, \Gamma_1, \dots, \Gamma_5)$  in  $\mathcal{V}$  where  $P = (I \ 0)$  and  $\bar{P}$  has a nonzero fourth column. If  $g \in G$  stabilizes  $v$ , then  $P = Pg$  and  $\bar{P} = \bar{P}g$  as elements of  $\mathcal{C}$ . Write  $g = \begin{pmatrix} \mathbf{R} & \mathbf{T} \\ 0 & \lambda \end{pmatrix}$ . From  $P = Pg$ , it follows  $\mathbf{R} = I$  and  $\mathbf{T} = 0$ . From  $\bar{P} = \bar{P}g$ , it follows  $\lambda = 1$ . Altogether  $g = I$ , so the stabilizer is trivial.

Next we show properness. By [6, Ch. 1, Sec. 10], this means  $\varphi : \mathcal{V} \times G \rightarrow \mathcal{V} \times \mathcal{V}$ ,  $(v, g) \mapsto (v, g \cdot v)$  is a closed map with compact fibers. By freeness (previous paragraph),  $\varphi$  is injective. So its fiber are either empty or singletons, hence compact. For closedness, we will prove the stronger property that  $\varphi$  is a homeomorphism onto its image and its image is a closed subset of  $\mathcal{V} \times \mathcal{V}$ . Note that the image of  $\varphi$  consists of all  $(v^{(1)}, v^{(2)}) \in \mathcal{V} \times \mathcal{V}$  with  $v^{(i)} = (P^{(i)}, \bar{P}^{(i)}, \Gamma_1^{(i)}, \dots, \Gamma_5^{(i)})$  where  $P^{(i)} = (\mathbf{R}^{(i)} \ \mathbf{T}^{(i)})$  and  $\bar{P}^{(i)} = (\bar{\mathbf{R}}^{(i)} \ \bar{\mathbf{T}}^{(i)})$  for  $i = 1, 2$  such that:

- i)  $(P^{(1)}, \bar{P}^{(1)})$  and  $(P^{(2)}, \bar{P}^{(2)})$  have the same essential matrix;
- ii)  $\mathbf{R}^{(1)}(\bar{\mathbf{R}}^{(1)})^\top = \mathbf{R}^{(2)}(\bar{\mathbf{R}}^{(2)})^\top$ ;
- iii)  $v^{(1)}$  and  $v^{(2)}$  map to the same image point pairs.

Indeed, this set contains  $\text{Im}(\varphi)$ , and the reverse containment follows from [26, Result 9.19]. In particular,  $\text{Im}(\varphi)$  is a closed subset of  $\mathcal{V} \times \mathcal{V}$ . For the homeomorphism claim, let  $\psi : \text{Im}(\varphi) \rightarrow \mathcal{V} \times G$  be the left-inverse of  $\varphi$ , which exists since  $\varphi$  is injective. Then  $\psi(v^{(1)}, v^{(2)}) = (v^{(1)}, g)$  for some  $g = \begin{pmatrix} \mathbf{R} & \hat{\mathbf{T}} \\ 0 & \lambda \end{pmatrix}$ . We need to show that  $g$  is a continuous function of  $(v^{(1)}, v^{(2)})$ . From  $P^{(1)} = P^{(2)}g$ , we see  $\mathbf{R} = \mathbf{R}^{(1)}(\mathbf{R}^{(2)})^\top$ , which is continuous. Using  $\bar{P}^{(1)} = \bar{P}^{(2)}g$ ,

$$\begin{pmatrix} P^{(2)} \\ \bar{P}^{(2)} \end{pmatrix} \begin{pmatrix} \mathbf{T} \\ \lambda \end{pmatrix} = \begin{pmatrix} \mathbf{T}^{(1)} \\ \mathbf{T}^{(2)} \end{pmatrix}. \quad (43)$$

The  $6 \times 4$  matrix in (43) is left-invertible, because  $P^{(2)}$  and  $\bar{P}^{(2)}$  have distinct centers. By [40, pg. 3], it follows that  $\mathbf{T}$  and  $\lambda$  are continuous functions of  $(v^{(1)}, v^{(2)}) \in \text{Im}(\varphi)$ , which concludes the verification of properness.

We now use the quotient manifold theorem [34, Thm. 21.10]. It gives a unique smooth structure on  $\mathcal{W} = \mathcal{V}/G$  such that the quotient map  $\mathcal{V} \rightarrow \mathcal{V}/G$  is a smooth submersion. From  $\dim(\mathcal{V}) = \dim(\mathcal{C}^{\times 2} \times (\mathbb{R}^3)^{\times 5}) = 2 \cdot 6 + 5 \cdot 3 = 27$  and  $\dim(G) = 7$ , we get  $\dim(\mathcal{W}) = 27 - 7 = 20$ .  $\square$

## APPENDIX B PROOF OF LEMMA M-2

Let the given map from  $\mathcal{U}$  to  $\mathcal{W}$  be  $\psi$ . Write  $\psi = \psi_2 \circ \psi_1$  where  $\psi_1 : \mathcal{U} \rightarrow \mathcal{V}$ ,  $\mathcal{V}$  is the open subset of  $\mathcal{C}^{\times 2} \times (\mathbb{R}^3)^{\times 5}$  in (M-1), and  $\psi : \mathcal{V} \rightarrow \mathcal{V}/G = \mathcal{W}$  is the quotient map.

We first check that  $\psi$  is surjective. Let  $v = (P, \bar{P}, \Gamma_1, \dots, \Gamma_5) \in \mathcal{V}$  where  $P = (\mathbf{R}_1 \ \mathbf{T}_1)$  and  $\bar{P} = (\mathbf{R}_2 \ \mathbf{T}_2)$ . We wish to show  $\text{im } \psi_1 \cap (G \cdot v) \neq \emptyset$ . Indeed,  $((I \ 0), (\mathbf{R} \ \hat{\mathbf{T}}), \frac{1}{\lambda}\Gamma_1, \dots, \frac{1}{\lambda}\Gamma_5)$  is in the intersection, where  $\mathbf{R} = \mathbf{R}_2\mathbf{R}_1^\top$ ,  $\hat{\mathbf{T}} = \frac{\mathbf{T}_2 - \mathbf{R}_2\mathbf{R}_1^\top\mathbf{T}_1}{\lambda}$  and  $\lambda = \|\mathbf{T}_2 - \mathbf{R}_2\mathbf{R}_1^\top\mathbf{T}_1\|_2$ .

Next we check that  $\psi$  is 2-to-1 everywhere. Assume  $u^{(i)} = (\mathbf{R}^{(i)}, \hat{\mathbf{T}}^{(i)}, \Gamma_1^{(i)}, \dots, \Gamma_5^{(i)})$  for  $i = 1, 2$  satisfy  $\psi(u^{(1)}) = \psi(u^{(2)})$ . Equivalently,  $\psi_1(u^{(1)})$  and  $\psi_1(u^{(2)})$  are in the same  $G$ -orbit, i.e. there exists  $g = \begin{pmatrix} \mathbf{R} & \hat{\mathbf{T}} \\ 0 & \lambda \end{pmatrix}$  such that

$$\begin{cases} (I \ 0) = (I \ 0)g \\ (\mathbf{R}^{(1)} \ \hat{\mathbf{T}}^{(1)}) = (\mathbf{R}^{(2)} \ \hat{\mathbf{T}}^{(2)})g \\ g(\Gamma_i^{(1)}; 1) = (\Gamma_i^{(2)}; 1) \end{cases}$$

The only possibilities are  $g = I$  and  $u^{(1)} = u^{(2)}$  or  $g = \text{diag}(1, 1, 1, -1)$  and  $(\mathbf{R}^{(2)}, \hat{\mathbf{T}}^{(2)}, \Gamma_1^{(2)}, \dots, \Gamma_5^{(2)}) = (\mathbf{R}^{(1)}, -\hat{\mathbf{T}}^{(1)}, -\Gamma_1^{(1)}, \dots, -\Gamma_5^{(1)})$  as desired.

Lastly we check that  $\psi$  is a submersion. Let  $u = (\mathbf{R}, \hat{\mathbf{T}}, \Gamma_1, \dots, \Gamma_5)$  and  $v = \psi_1(u)$ . It is easy to see

$$\text{im } D\psi_1(u) = 0 \times \{([\dot{s}] \times \mathbf{R} \ \dot{\alpha}_1 \mathbf{T}_1^\top + \dot{\alpha}_2 \mathbf{T}_2^\top) : \dot{s} \in \mathbb{R}^3, \dot{\alpha} \in \mathbb{R}^2\} \times (\mathbb{R}^3)^{\times 5} \quad (44)$$

using facts (83), (84), (86) below. On the other hand, by Proposition M-1,

$$\ker D\psi_2(v) = T(G \cdot v, v). \quad (45)$$

A chain rule computation shows

$$T(G \cdot v, v) = \left\{ \left( -([\dot{s}] \times \hat{\mathbf{T}}), \frac{-1}{2}(\mathbf{R}[\dot{s}] \times \mathbf{R}\hat{\mathbf{T}} + \dot{\lambda}\hat{\mathbf{T}})^\perp, \dots, [\dot{s}] \times \Gamma_i + \hat{\mathbf{T}} - \dot{\lambda}\Gamma_i, \dots \right) : s \in \mathbb{R}^3, \dot{\mathbf{T}} \in \mathbb{R}^3, \dot{\lambda} \in \mathbb{R} \right\}, \quad (46)$$

where “ $\perp$ ” indicates the component orthogonal to  $(\mathbf{R} \ \hat{\mathbf{T}})$  and we’re identifying  $T(\mathcal{C}, (\mathbf{R} \ \hat{\mathbf{T}}))$  with a subspace of  $T(\mathbb{P}(\mathbb{R}^{3 \times 4}), (\mathbf{R} \ \hat{\mathbf{T}})) = (\mathbb{R}^{3 \times 4})^\perp$  (see Section L.4 below). Comparing (44), (45), (46), one verifies

$$\text{im } D\psi_1(u) \cap \ker D\psi_2(v) = 0.$$

Further, clearly  $D\psi_1(u)$  has rank  $\dim(\mathcal{U}) = \dim(\mathcal{W})$ . As wanted,  $D\psi(u) = D\psi_2(v) \circ D\psi_1(u)$  is surjective.

By [34, Cor. 4.13], we have proven that  $\psi$  is a smooth double cover of  $\mathcal{W}$ .  $\square$

## APPENDIX C PROOF OF PROPOSITION M-3

Let  $\mathcal{V}$  be the open subset of  $\mathcal{C}^{\times 2} \times (\mathbb{P}_{\mathbb{R}}^3)^{\times 7}$  in (M-8).

The action (M-9) is clearly smooth.

For freeness, note that each orbit contains a point  $v = (P, \bar{P}, \hat{\Gamma}_1, \dots, \hat{\Gamma}_7)$  where  $P = (I \ 0)$  and  $\bar{P} = (\mathbf{p}_1 \ \mathbf{p}_2 \ \mathbf{p}_3 \ \mathbf{p}_4)$  with  $\mathbf{p}_4 \neq 0$ . Let  $g \in \text{PGL}(4)$  stabilize  $v$ . From  $P = Pg$ ,

$$g = \begin{pmatrix} 1 & 0 & 0 & 0 \\ 0 & 1 & 0 & 0 \\ 0 & 0 & 1 & 0 \\ g_{41} & g_{42} & g_{43} & g_{44} \end{pmatrix} \quad (47)$$

where  $g_{44} \neq 0$ . From  $\bar{P} = \bar{P}g$ , get  $\mathbf{p}_i + g_{4i}\mathbf{p}_4 = g_{44}\mathbf{p}_i$  in  $\mathbb{R}^3$  for  $i = 1, 2, 3$ . If  $g_{44} \neq 1$  then  $\mathbf{p}_i = \frac{g_{4i}}{g_{44}-1}\mathbf{p}_4$  for  $i = 1, 2, 3$ . Then  $\text{rank}(\bar{P}) = 1$ , contradicting  $\text{rank } \bar{P} = 3$ . Thus  $g_{44} = 1$ , implying  $g_{4i} = 0$  for  $i = 1, 2, 3$ . Therefore  $g = I$ , and the stabilizer is trivial.

Next consider properness, or equivalently that  $\varphi : \mathcal{V} \times \text{PGL}(4) \rightarrow \mathcal{V} \times \mathcal{V}$ ,  $(v, g) \mapsto (v, g \cdot v)$  is a closed map with compact fibers. By freeness,  $\varphi$  is injective; in particular its fibers are compact. For closedness, we show that  $\varphi$  is a homeomorphism onto its image and  $\text{Im}(\varphi)$  is a closed subset of  $\mathcal{V} \times \mathcal{V}$ . By [26, Thm. 9.10], the image consists of all pairs  $(v^{(1)}, v^{(2)}) \in \mathcal{V} \times \mathcal{V}$  with  $v^{(i)} = (P^{(i)}, \bar{P}^{(i)}, \hat{\Gamma}_1^{(i)}, \dots, \hat{\Gamma}_7^{(i)})$  for  $i = 1, 2$  such that:

- i)  $(P^{(1)}, \bar{P}^{(1)})$  and  $(P^{(2)}, \bar{P}^{(2)})$  have the same fundamental matrix;
- ii)  $v^{(1)}$  and  $v^{(2)}$  map to the same image point pairs in  $(\mathbb{R}^2 \times \mathbb{R}^2)^{\times 7}$ .

For the homeomorphism claim, let  $\psi : \text{Im}(\varphi) \rightarrow \mathcal{V} \times \text{PGL}(4)$  be the left-inverse of  $\varphi$ , which exists since  $\varphi$  is injective. Then  $\psi(v^{(1)}, v^{(2)}) = (v^{(1)}, g)$  for  $g \in \text{PGL}(4)$ . We need to show that  $g$  is a continuous function of  $(v^{(1)}, v^{(2)})$ . Note

$$\begin{cases} P^{(1)} = P^{(2)}g \\ \bar{P}^{(1)} = \bar{P}^{(2)}g \end{cases} \quad (48)$$

as elements of  $\mathcal{C}$ . Regard this as a linear system in  $g$ , where the invertibility of  $g$  is temporarily relaxed. Namely, since the equalities in (48) are up to scale, we require that the  $2 \times 2$  minors of  $(\text{vec}(P^{(1)}) \ \text{vec}(P^{(2)}g))$  and





If  $(\dot{s}, \dot{\alpha}) \neq 0$ , it's easy to see  $Q(\dot{s}, \dot{\alpha})$  corresponds to a quadric surface  $\mathcal{Q}$  in  $\mathbb{R}^3$  containing the baseline  $\text{span}(\mathbf{R}^\top \hat{\mathbf{T}})$ , and meeting any plane perpendicular to the baseline in a circle. Conversely, all such  $\mathcal{Q}$  come from a matrix  $Q(\dot{s}, \dot{\alpha})$  with  $(\dot{s}, \dot{\alpha}) \neq 0$ . Lastly, note (67) says that  $\mathcal{Q}$  passes through  $\Gamma_i$  ( $i = 1, \dots, 5$ ). Therefore Theorem M-18 follows.  $\square$

## APPENDIX H PROOF OF THEOREM M-19

Let  $w = (b, \Gamma_1, \dots, \Gamma_7) \in \mathcal{W}$ . Let  $\Delta = (\dot{b}, \dot{\Gamma}_1, \dots, \dot{\Gamma}_7)$  represent an element of  $T(\mathcal{W}, w)$ , expressed in terms of the ordered basis (58) where  $\dot{b} \in \mathbb{R}^7$  and  $\dot{\Gamma}_i \in \mathbb{R}^3$ . We need to characterize world scenes such that

$$D\Phi_1(w)\Delta \in \ker D\Phi_2(\Phi_1(w)) \quad (68)$$

for some nonzero  $\Delta$ , where  $D\Phi_1$  and  $D\Phi_2$  are as in Proposition M-17.

Like in the proof of Theorem M-18,

$$\ker D\Phi_2(\Phi_1(w)) = \mathbb{R}\Gamma_1 \oplus \dots \oplus \mathbb{R}\Gamma_7 \oplus \mathbb{R}(\mathbf{M}(b)(\Gamma_i; 1)) \oplus \dots$$

By the form of  $D\Phi_1(w)$  in Fig. 16, (68) is equivalent to

$$\begin{cases} \dot{\Gamma}_i = \lambda_i \Gamma_i \\ D\mathbf{M}(b)(\dot{b})(\Gamma_i; 1) + \mathbf{M}(b)(\dot{\Gamma}_i; 0) = \mu_i (\mathbf{M}(b)(\Gamma_i; 1)) \end{cases} \quad (69)$$

for  $i = 1, \dots, 7$ , some  $\lambda, \mu \in \mathbb{R}^7$  and

$$D\mathbf{M}(b)(\dot{b}) = \begin{pmatrix} 0 & \dot{b}_1 & \dot{b}_2 & \dot{b}_3 \\ \dot{b}_4 & \dot{b}_5 & \dot{b}_6 & \dot{b}_7 \\ 0 & 0 & 0 & 0 \end{pmatrix}.$$

Equating third coordinates in the bottom line of (69), it must be that  $\mu = 0$  as  $(\mathbf{M}(b)(\Gamma_i; 1))_3 \neq 0$  for  $i = 1, \dots, 7$ . Substituting the top line of (69) into the bottom line gives

$$\begin{pmatrix} 0 & \dot{b}_1 & \dot{b}_2 & \dot{b}_3 \\ \dot{b}_4 & \dot{b}_5 & \dot{b}_6 & \dot{b}_7 \end{pmatrix} \begin{pmatrix} \Gamma_i \\ 1 \end{pmatrix} + \lambda_i \begin{pmatrix} 1 & b_1 & b_2 \\ b_4 & b_5 & b_6 \end{pmatrix} \Gamma_i = 0 \quad (70)$$

for  $i = 1, \dots, 7$ . The task is to characterize when (70) has a nonzero solution in  $\dot{b}, \lambda$  (the justification that this is equivalent is like in the proof of Theorem M-19).

We now eliminate  $\lambda_i$ , by multiplying (70) on the left by

$$\begin{pmatrix} -b_4(\Gamma_i)_1 - b_5(\Gamma_i)_2 - b_6(\Gamma_i)_3 \\ (\Gamma_i)_1 + b_1(\Gamma_i)_2 + b_2(\Gamma_i)_3 \end{pmatrix}^\top$$

which kills  $\begin{pmatrix} 1 & b_1 & b_2 \\ b_4 & b_5 & b_6 \end{pmatrix} \Gamma_i$ . The resulting linear system in  $\dot{b}$  is

$$\begin{pmatrix} -b_4(\Gamma_i)_1(\Gamma_i)_2 - b_5(\Gamma_i)_2^2 - b_6(\Gamma_i)_2(\Gamma_i)_3 \\ -b_4(\Gamma_i)_1(\Gamma_i)_3 - b_5(\Gamma_i)_2(\Gamma_i)_3 - b_6(\Gamma_i)_3^2 \\ -b_4(\Gamma_i)_1 - b_5(\Gamma_i)_2 - b_6(\Gamma_i)_3 \\ (\Gamma_i)_1^2 + b_1(\Gamma_i)_1(\Gamma_i)_2 + b_2(\Gamma_i)_1(\Gamma_i)_3 \\ (\Gamma_i)_1(\Gamma_i)_2 + b_1(\Gamma_i)_2^2 + b_2(\Gamma_i)_2(\Gamma_i)_3 \\ (\Gamma_i)_1(\Gamma_i)_3 + b_1(\Gamma_i)_2(\Gamma_i)_3 + b_2(\Gamma_i)_3^2 \\ (\Gamma_i)_1 + b_1(\Gamma_i)_2 + b_2(\Gamma_i)_3 \end{pmatrix}^\top \dot{b} = 0 \quad (71)$$

for  $i = 1, \dots, 7$ . Then (71) has a nonzero solution if and only if (70) does (the proof of this is similar as for Theorem M-19).

Let us now interpret (71) geometrically. Rewrite it as

$$\begin{pmatrix} \Gamma_i \\ 1 \end{pmatrix}^\top Q(\dot{b}) \begin{pmatrix} \Gamma_i \\ 1 \end{pmatrix} = 0 \quad (72)$$

for  $i = 1, \dots, 7$ , where  $Q(\dot{b}) := \dot{b}_1 Q_1 + \dots + \dot{b}_7 Q_7$  and

$$Q_1 = \begin{pmatrix} 0 & -b_4 & 0 & 0 \\ -b_4 & -2b_5 & -b_6 & 0 \\ 0 & -b_6 & 0 & 0 \\ 0 & 0 & 0 & 0 \end{pmatrix}, \quad Q_2 = \begin{pmatrix} 0 & 0 & -b_4 & 0 \\ 0 & 0 & -b_5 & 0 \\ -b_4 & -b_5 & -2b_6 & 0 \\ 0 & 0 & 0 & 0 \end{pmatrix}$$

$$Q_3 = \begin{pmatrix} 0 & 0 & 0 & -b_4 \\ 0 & 0 & 0 & -b_5 \\ 0 & 0 & 0 & -b_6 \\ -b_4 & -b_5 & -b_6 & 0 \end{pmatrix}, \quad Q_4 = \begin{pmatrix} 2 & b_1 & b_2 & 0 \\ b_1 & 0 & 0 & 0 \\ b_2 & 0 & 0 & 0 \\ 0 & 0 & 0 & 0 \end{pmatrix}$$

$$Q_5 = \begin{pmatrix} 0 & 1 & 0 & 0 \\ 1 & 2b_1 & b_2 & 0 \\ 0 & b_2 & 0 & 0 \\ 0 & 0 & 0 & 0 \end{pmatrix}, \quad Q_6 = \begin{pmatrix} 0 & 0 & 1 & 0 \\ 0 & 0 & b_1 & 0 \\ 1 & b_1 & 2b_2 & 0 \\ 0 & 0 & 0 & 0 \end{pmatrix}$$

$$Q_7 = \begin{pmatrix} 0 & 0 & 0 & 1 \\ 0 & 0 & 0 & b_1 \\ 0 & 0 & 0 & b_2 \\ 1 & b_1 & b_2 & 0 \end{pmatrix}.$$

It remains to prove that  $Q_1, \dots, Q_7$  form a basis for the subspace of  $\text{Sym}^2(\mathbb{R}^4)$  corresponding to all quadrics  $\mathcal{Q}$  containing the baseline. Clearly this will imply Theorem M-19, because (72) says  $\mathcal{Q}$  passes through  $\Gamma_1, \dots, \Gamma_7$ .

Note that the subspace in question has dimension 7, since containing a line is 3 linearly independent conditions. Further, by direct calculation (Cramer's rule) the baseline is

$$\text{span}(b_2 b_5 - b_1 b_6 \quad -b_2 b_4 + b_6 \quad b_1 b_4 - b_5)^\top \subseteq \mathbb{R}^3. \quad (73)$$

It's easy to check the quadrics corresponding to  $Q_i$  contain (73). So we are done if  $Q_1, \dots, Q_7$  are linearly independent.

Assume  $Q(\dot{b}) = 0$ . Comparing top-left entries,  $\dot{b}_4 = 0$ . Comparing bottom rows and rightmost columns,

$$\begin{pmatrix} 1 & b_1 & b_2 \\ b_4 & b_5 & b_6 \end{pmatrix} \begin{pmatrix} \dot{b}_7 \\ -\dot{b}_3 \end{pmatrix} = 0. \quad (74)$$

It implies  $\dot{b}_3 = \dot{b}_7 = 0$ , because  $\mathbf{M}(b)(1 : 2, 1 : 3)$  must be rank-2 if  $\mathbf{M}(b)$  is rank-3. Next define

$$\tilde{Q} := \dot{b}_1 Q_1 + \dot{b}_5 Q_5 = -\dot{b}_2 Q_2 - \dot{b}_6 Q_6. \quad (75)$$

Given the supports of  $Q_i$ ,  $\tilde{Q} = \lambda(e_2 e_3^\top + e_3 e_2^\top)$  for some  $\lambda \in \mathbb{R}$ . Further, (75) reshapes to

$$\begin{pmatrix} \dot{b}_5 & -\dot{b}_1 \end{pmatrix} \begin{pmatrix} 1 & 2b_1 & b_2 \\ b_4 & 2b_5 & b_6 \end{pmatrix} = \begin{pmatrix} 0 & 0 & \lambda \end{pmatrix} \quad (76)$$

and

$$\begin{pmatrix} \dot{b}_6 & -\dot{b}_2 \end{pmatrix} \begin{pmatrix} 1 & b_1 & 2b_2 \\ b_4 & b_5 & 2b_6 \end{pmatrix} = \begin{pmatrix} 0 & \lambda & 0 \end{pmatrix}. \quad (77)$$

If  $\lambda \neq 0$ , we can deduce that  $\begin{pmatrix} 1 & b_1 & b_2 \\ b_4 & b_5 & b_6 \end{pmatrix}$  has row-space  $\text{span}(e_2, e_3)$ , which is absurd. Hence  $\lambda = 0$ . Then similarly to (74), (76) implies  $\dot{b}_1 = \dot{b}_5 = 0$  and (77) implies  $\dot{b}_2 = \dot{b}_6 = 0$ . We've shown  $\dot{b} = 0$ , hence  $Q_1, \dots, Q_7$  are linearly independent.

The proof of Theorem M-18 is complete. Note that a similar argument shows the analogous result if the world scene lives in a different chart from Lemma M-4.  $\square$

## APPENDIX I

### PROOF OF THEOREM M-20

Given the sketch, it remains only to verify the property from Proposition M-15.

Let  $x = ((\gamma_1, \bar{\gamma}_1), \dots, (\gamma_5, \bar{\gamma}_5)) \in \mathcal{X} \setminus \text{disc}(\mathcal{M}, \mathbf{L})$ ,  $E \in \mathcal{Y} \cap \ker \mathbf{L}(x)$ , and  $w = ((I \ 0), (\mathbf{R} \ \hat{\mathbf{T}}), \Gamma_1, \dots, \Gamma_5) \in \Psi^{-1}(E) \cap \Phi^{-1}(x)$ . In terms of  $E$ , there are four possibilities for  $(\mathbf{R}, \hat{\mathbf{T}}) \in \text{SO}(3) \times \mathbb{S}^2$ , see [26, Result 9.19]. (Only two are distinct up to the action of  $G$ , see the comment after Lemma M-2.) Further, the explicit formulas for  $(\mathbf{R}, \hat{\mathbf{T}})$  in [26, Result 9.19] are smooth functions of  $E$ 's SVD factors. Shrinking  $\mathcal{X}_0$  and  $\mathcal{Y}_0$  if necessary,  $E$ 's SVD factors can be chosen as smooth functions of the essential matrix, even though  $E$  has repeated singular values. Indeed, it is possible because

$$\text{SO}(3) \times \text{SO}(3) \rightarrow \mathcal{Y}, \quad (\mathbf{R}_1, \mathbf{R}_2) \mapsto \mathbf{R}_1 \text{diag}(1, 1, 0) \mathbf{R}_2^\top$$

is an  $\text{SO}(2) \times (\mathbb{Z}/2\mathbb{Z})^{\times 2}$ -smooth bundle map, see [49]. It follows that  $\mathbf{R}$  and  $\hat{\mathbf{T}}$  locally extend to smooth functions of  $E$ , thus to smooth functions of the image data  $x$  through  $f$  from Lemma M-14. More precisely, there exists a smooth function  $h_1 : \mathcal{X}_0 \rightarrow \text{SO}(3) \times \mathbb{S}^2$  such that  $h_1(x) = (\mathbf{R}, \hat{\mathbf{T}})$  and  $((\mathbf{R}', \hat{\mathbf{T}}') \mapsto [\hat{\mathbf{T}}']_{\times} \mathbf{R}') \circ h_1 = f$  as wanted.

As for the world points, because  $\Phi(w) = x$ , they satisfy

$$\begin{cases} (I \ 0)(\Gamma_i; 1) = (\gamma_i; 1) \\ (\mathbf{R} \ \hat{\mathbf{T}})(\Gamma_i; 1) = (\bar{\gamma}_i; 1). \end{cases} \quad (78)$$

Further  $\Gamma_i$  are uniquely determined by (78), provided the backprojections

$$(I \ 0)^{-1}(\gamma_i; 1) \subseteq \mathbb{P}_{\mathbb{R}}^3 \quad \text{and} \quad (\mathbf{R} \ \hat{\mathbf{T}})^{-1}(\bar{\gamma}_i; 1) \subseteq \mathbb{P}_{\mathbb{R}}^3 \quad (79)$$

are distinct lines. In this case,  $\Gamma_i$  locally extend to smooth functions of the image data  $x$ . Indeed, the world points are determined by (78), where  $(\gamma_i, \bar{\gamma}_i)$  are replaced by  $(\gamma'_i, \bar{\gamma}'_i)$  varying in  $\mathcal{X}_0$  and  $(\mathbf{R} \ \hat{\mathbf{T}})$  is replaced by  $h_1((\gamma'_1, \bar{\gamma}'_1), \dots, (\gamma'_5, \bar{\gamma}'_5))$ . More precisely, after possibly shrinking  $\mathcal{X}_0$  again, there is a smooth map  $h_2 : \mathcal{X}_0 \rightarrow (\mathbb{R}^3)^{\times 5}$  such that  $h(x') := ((I \ 0), h_1(x'), h_2(x')) \in \mathcal{W}$  for  $x' \in \mathcal{X}_0$  satisfies the requirements in the smooth lifting property.

To finish, we just need to argue that (79) are distinct lines. For a contradiction, suppose not. Then both lines are the baseline. So  $\gamma_i$  and  $\bar{\gamma}_i$  are the epipoles, i.e.  $(\gamma_i; 1) = \mathbf{R}^\top \hat{\mathbf{T}}$  and  $(\bar{\gamma}_i; 1) = \hat{\mathbf{T}}$  in  $\mathbb{P}_{\mathbb{R}}^3$ . But the corresponding epipolar constraint is now orthogonal to  $T(\mathcal{Y}, E)$ . This is because

$$\hat{\mathbf{T}}^\top ([\hat{\mathbf{T}}^\perp]_{\times} \mathbf{R}) \mathbf{R}^\top \hat{\mathbf{T}} = \hat{\mathbf{T}}^\top [\hat{\mathbf{T}}^\perp]_{\times} \hat{\mathbf{T}} = 0$$

for  $i = 1, 2$ , and

$$\hat{\mathbf{T}}^\top ([\hat{\mathbf{T}}]_{\times} [\hat{s}]_{\times} \mathbf{R}) \mathbf{R}^\top \hat{\mathbf{T}} = (\hat{\mathbf{T}}^\top [\hat{\mathbf{T}}]_{\times}) [\hat{s}]_{\times} \mathbf{R} \mathbf{R}^\top \hat{\mathbf{T}} = 0$$

for all  $\hat{s} \in \mathbb{R}^3$ . It implies  $\mathcal{Y} \cap \ker \mathbf{L}(x)$  in  $\mathbb{P}(\mathbb{R}^{3 \times 3})$  is not traverse at  $E$ , contradicting  $x \notin \text{disc}(\mathcal{M}, \mathbf{L})$ .  $\square$

## APPENDIX J

### PROOF OF THEOREM M-22

We only need to verify the smooth lifting property.

Let  $x = ((\gamma_1, \bar{\gamma}_1), \dots, (\gamma_7, \bar{\gamma}_7)) \in \mathcal{X} \setminus \text{disc}(\mathcal{M}, \mathbf{L})$ ,  $F \in \mathcal{Y} \cap \ker \mathbf{L}(x)$ , and  $w = ((I \ 0), \bar{P}, \tilde{\Gamma}_1, \dots, \tilde{\Gamma}_7) \in \Psi^{-1}(F) \cap \Phi^{-1}(x)$ . In terms of  $F$ , there is only one possibility for  $\bar{P}$  up

to the action of  $\text{PGL}(4)$ , see [26, Result 9.14]. The explicit formula for  $\bar{P}$  in [26, Result 9.14] is a smooth function of  $F$ , since the epipole in  $\mathbb{P}_{\mathbb{R}}^2$  is a smooth function of  $F \in \mathcal{Y}$ . So  $\bar{P}$  extends to a smooth function of  $F$ , thus to a smooth function of the image data  $x$  as wanted.

The argument for the world points  $\tilde{\Gamma}_i$  is similar to the one for Theorem M-20. Again we need to check  $(I \ 0)^{-1}(\gamma_i; 1)$  and  $\bar{P}^{-1}(\bar{\gamma}_i; 1)$  are distinct lines. Supposing not, both are the baseline. Then  $(\gamma_i; 1)$  and  $(\bar{\gamma}_i; 1)$  are the epipoles. Their outer product is orthogonal to  $T(\mathcal{Y}, F)$  by Lemma 29 below. Thus  $\mathcal{Y} \cap \ker \mathbf{L}(x) \subseteq \mathbb{P}(\mathbb{R}^{3 \times 3})$  isn't traverse at  $F$ , contradicting  $x \notin \text{disc}(\mathcal{M}, \mathbf{L})$ .  $\square$

## APPENDIX K

### PROOF OF PROPOSITION M-26

Consider the uncalibrated case. Let  $w'$  be represented  $(P, \bar{P}, \tilde{\Gamma}_1, \dots, \tilde{\Gamma}_N) \in \mathcal{C}^{\times 2} \times (\mathbb{P}_{\mathbb{R}}^3)^{\times N}$  where  $N \geq 7$ . As explained in the main paper, it suffices to show that there exists a common quadric  $\mathcal{Q}$  satisfying the conditions of Theorem M-19 for each minimal subscene  $w$  of  $w'$ .

Let  $Q \in S^2(\mathbb{R}^4)$  be a nonzero  $4 \times 4$  real symmetric matrix corresponding to the quadric surface  $\mathcal{Q}$  in  $\mathbb{P}_{\mathbb{R}}^3$ . For different choices of  $w$ , the second bullet in Theorem M-19 is the same. The set of  $Q$ 's satisfying the condition is a codimension-3 linear subspace of  $S^2(\mathbb{R}^4)$ . Parameterize it as

$$\{Q(\alpha) = \alpha_1 Q_1 + \dots + \alpha_7 Q_7 : \alpha \in \mathbb{R}^7\}$$

where  $Q_i$  form a fixed basis.

For a minimal subscene  $w$ , the first bullet in Theorem M-18 reads:

$$\tilde{\Gamma}_i^\top Q(\alpha) \tilde{\Gamma}_i = 0 \quad \text{for each } \tilde{\Gamma}_i \text{ in } w, \quad (80)$$

By assumption, (80) has a nonzero solution in  $\alpha$ . Varying  $w$ , it means that if we consider the  $N \times 7$  linear system:

$$M\alpha = 0, \quad \text{where } M_{ij} := \tilde{\Gamma}_i^\top Q_j \tilde{\Gamma}_i, \quad (81)$$

then each  $7 \times 7$  subsystem has a nonzero solution. We deduce that  $M \in \mathbb{R}^{N \times 7}$  has rank at most 6, so (81) has a nonzero solution. The corresponding quadric surface does the job.

The calibrated case in Proposition M-26 is nearly same. The differences are that second and third bullets in Theorem M-18 define a codimension-5 subspace of  $S^2(\mathbb{R}^4)$ , and (81) is now an  $N \times 5$  linear system of rank at most 4.  $\square$

## APPENDIX L

### BACKGROUND ON MANIFOLDS

We list the tangent spaces and (where relevant) Riemannian metrics for the manifolds used in this paper. Recall that in our framework for the condition number, the input and output spaces need to be Riemannian manifolds, while for the world scene space only the smooth structure is relevant.

#### L.1 Image data spaces

Consider  $\mathcal{X} = (\mathbb{R}^2 \times \mathbb{R}^2)^{\times n}$  where  $n = 5$  or  $7$ . Then  $\mathcal{X} \cong \mathbb{R}^{4n}$ . The tangent spaces are all canonically isomorphic to  $\mathbb{R}^{4n}$ . The inner products on the tangent spaces are all the Euclidean inner product.

## L.2 World scene space for 5-point problem

Consider  $\mathcal{W}$  from Proposition M-1. By Lemma M-2, an open dense subset of  $\text{SO}(3) \times \mathbb{S}^2 \times (\mathbb{R}^3)^{\times 5}$  is a smooth double cover of  $\mathcal{W}$ . It induces isomorphisms on tangent spaces:

$$T(\mathcal{W}, ((I \ 0), (\mathbf{R} \ \hat{\mathbf{T}}), \Gamma_1, \dots, \Gamma_5)) \cong T(\text{SO}(3), \mathbf{R}) \times T(\mathbb{S}^2, \hat{\mathbf{T}}) \times (\mathbb{R}^3)^{\times 5}. \quad (82)$$

The tangent spaces to  $\text{SO}(3)$  are

$$T(\text{SO}(3), \mathbf{R}) = \{[\dot{s}]_{\times} \mathbf{R} : \dot{s} \in \mathbb{R}^3\}, \quad (83)$$

where  $[\dot{s}]_{\times} := \begin{pmatrix} 0 & -\dot{s}_3 & \dot{s}_2 \\ \dot{s}_3 & 0 & -\dot{s}_1 \\ -\dot{s}_2 & \dot{s}_1 & 0 \end{pmatrix}$  for  $\dot{s} = \begin{pmatrix} \dot{s}_1 \\ \dot{s}_2 \\ \dot{s}_3 \end{pmatrix}$ . A basis for  $T(\text{SO}(3), \mathbf{R})$  is  $[e_1]_{\times} \mathbf{R}$ ,  $[e_2]_{\times} \mathbf{R}$ ,  $[e_3]_{\times} \mathbf{R}$ , where  $e_1, e_2, e_3$  is the standard basis on  $\mathbb{R}^3$ . The tangent spaces to  $\mathbb{S}^2$  are

$$T(\mathbb{S}^2, \hat{\mathbf{T}}) = \{\dot{\mathbf{T}} \in \mathbb{R}^3 : \langle \dot{\mathbf{T}}, \hat{\mathbf{T}} \rangle = 0\}. \quad (84)$$

We let  $\hat{\mathbf{T}}_1^{\perp}, \hat{\mathbf{T}}_2^{\perp}$  denote an orthonormal basis of  $T(\mathbb{S}^2, \hat{\mathbf{T}})$ .

## L.3 World scene space for 7-point problem

Consider  $\mathcal{W}$  from Proposition M-3. Lemma M-4 describes an atlas for  $\mathcal{W}$ . The parameterizations there induce isomorphisms on tangent spaces:

$$T(\mathcal{W}, ((I \ 0), \mathbf{M}(b), \tilde{\Gamma}_1, \dots, \tilde{\Gamma}_7)) \cong \mathbb{R}^7 \times (\mathbb{R}^3)^{\times 7}. \quad (85)$$

## L.4 Projective space

Consider  $\mathbb{P}(\mathbb{R}^{3 \times 3})$ , the projective space of real  $3 \times 3$  matrices, in which essential and fundamental matrices live. The map:

$$\mathbb{S}^8 = \{M \in \mathbb{R}^{3 \times 3} : \|M\|_F = 1\} \rightarrow \mathbb{P}(\mathbb{R}^{3 \times 3}), \quad M \mapsto M,$$

sending a unit-Frobenius norm matrix to its projective point expresses  $\mathbb{P}(\mathbb{R}^{3 \times 3})$  as a quotient of  $\mathbb{S}^8$  by  $\mathbb{Z}/2\mathbb{Z}$ . Here  $\mathbb{Z}/2\mathbb{Z}$  acts by sending  $M$  to  $-M$ , which is an isometry. So  $\mathbb{P}(\mathbb{R}^{3 \times 3})$  inherits a Riemannian structure such that the quotient map is a local isometry [33, Exam. 2.34 and Prop. 2.32]. Therefore,

$$T(\mathbb{P}(\mathbb{R}^{3 \times 3}), M) \cong T(\mathbb{S}^8, M/\|M\|_F) = \{\dot{M} \in \mathbb{R}^{3 \times 3} : \langle \dot{M}, M \rangle = 0\}, \quad (86)$$

with inner product the restriction of the Frobenius inner product. An analogous Riemannian structure exists on other projective spaces, such as  $\mathbb{P}(\mathbb{R}^{3 \times 4})$  where cameras live.

## L.5 Output space for 5-point problem

Consider  $\mathcal{Y} = \mathcal{E} \subseteq \mathbb{P}(\mathbb{R}^{3 \times 3})$ , the manifold of real essential matrices from (M-4). It is known that  $\mathcal{E}$  is a compact Riemannian manifold of dimension 5. Its Riemannian metric is inherited from  $\mathbb{P}(\mathbb{R}^{3 \times 3})$ , *i.e.* the inner products on tangent spaces to  $\mathcal{E}$  are restrictions of the Frobenius inner product on (86). Its tangent spaces are characterized by the next lemma.

**Lemma 27.** The parameterization

$$\text{SO}(3) \times \mathbb{S}^2 \rightarrow \mathcal{E}, \quad (\mathbf{R}, \hat{\mathbf{T}}) \mapsto [\hat{\mathbf{T}}]_{\times} \mathbf{R}$$

is submersion, *i.e.* its differential has rank 5 everywhere.

**Proof:** At  $(\mathbf{R}, \hat{\mathbf{T}})$ , the differential sends  $([\dot{s}]_{\times} \mathbf{R}, \dot{\mathbf{T}})$  to

$$[\dot{\mathbf{T}}]_{\times} \mathbf{R} + [\hat{\mathbf{T}}]_{\times} [\dot{s}]_{\times} \mathbf{R}.$$

Assume this equals zero. Left-multiplying by  $\hat{\mathbf{T}}$  and using (84), it follows  $\dot{\mathbf{T}} = 0$ . Right-multiplying by  $\mathbf{R}^{\top}$ , we get

$$[\hat{\mathbf{T}}]_{\times} [\dot{s}]_{\times} = 0.$$

Since  $[\hat{\mathbf{T}}]_{\times}$  has rank 2,  $[\dot{s}]_{\times}$  has rank at most 1. It follows that  $\dot{s} = 0$ , and so the differential is injective.  $\square$

It follows that the tangent spaces to  $\mathcal{E}$  are

$$T(\mathcal{E}, [\hat{\mathbf{T}}]_{\times} \mathbf{R}) = \{[\dot{\mathbf{T}}]_{\times} \mathbf{R} + [\hat{\mathbf{T}}]_{\times} [\dot{s}]_{\times} \mathbf{R} : \dot{\mathbf{T}} \in \mathbb{R}^3, \langle \dot{\mathbf{T}}, \hat{\mathbf{T}} \rangle = 0, \dot{s} \in \mathbb{R}^3\}. \quad (87)$$

A non-orthonormal basis for  $T(\mathcal{E}, [\hat{\mathbf{T}}]_{\times} \mathbf{R})$  is

$$[\hat{\mathbf{T}}]_{\times} [e_1]_{\times} \mathbf{R}, [\hat{\mathbf{T}}]_{\times} [e_2]_{\times} \mathbf{R}, [\hat{\mathbf{T}}]_{\times} [e_3]_{\times} \mathbf{R}, [\hat{\mathbf{T}}_1^{\perp}]_{\times} \mathbf{R}, [\hat{\mathbf{T}}_2^{\perp}]_{\times} \mathbf{R}. \quad (88)$$

Orthonormalizing this gives an orthonormal basis. Specifically, we pass between bases using a linear algebra fact:

**Lemma 28.** Let  $X \in \mathbb{R}^{n \times d}$  have linearly independent columns, and  $z = X\alpha$  for  $\alpha \in \mathbb{R}^d$ . Define  $G = X^{\top} X \in \mathbb{R}^{d \times d}$  as the Gram matrix. Then  $Y = XG^{-1/2} \in \mathbb{R}^{n \times d}$  has orthonormal columns which form a basis for the column space of  $X$ , and  $z = Y\beta$  for  $\beta = G^{1/2}\alpha \in \mathbb{R}^d$ .

**Proof:** Let  $X = U\Sigma V^{\top}$  be a thin SVD. Then  $G = V\Sigma^2 V^{\top}$ ,  $(X^{\top} X)^{-1/2} = V\Sigma^{-1} V^{\top}$  and  $Y = UV^{\top}$ . Clearly  $Y$  has orthonormal columns which form a basis for the column space of  $X$ . The statement involving  $\beta$  is also immediate.  $\square$

Consequently if  $\alpha \in \mathbb{R}^5$  represents an element of  $T(\mathcal{E}, [\hat{\mathbf{T}}]_{\times} \mathbf{R})$  with respect to (88), then  $\beta = G^{1/2}\alpha \in \mathbb{R}^5$  represents the same element with respect to an orthonormal basis. Here  $G$  is the Gram matrix associated to (88), explicitly shown in Fig. 15.

## L.6 Output space for 7-point problem

Consider  $\mathcal{Y} = \mathcal{F} \subseteq \mathbb{P}(\mathbb{R}^{3 \times 3})$ , the manifold of real fundamental matrices. It is known that  $\mathcal{F}$  is a non-compact Riemannian manifold of dimension 7. Its Riemannian metric is inherited from  $\mathbb{P}(\mathbb{R}^{3 \times 3})$ . Its tangent spaces are as follows.

**Lemma 29.** Let  $F \in \mathcal{F} \subseteq \mathbb{P}(\mathbb{R}^{3 \times 3})$ . Using the identification (86), the tangent space to  $\mathcal{F}$  is

$$T(\mathcal{F}, F) = \{\dot{M} \in \mathbb{R}^{3 \times 3} : \langle \dot{M}, F \rangle = 0, \mathbf{e}'^{\top} \dot{M} \mathbf{e} = 0\}, \quad (89)$$

where  $\mathbf{e}, \mathbf{e}'$  are the right and left epipoles of  $F$  respectively.

**Proof:** The determinant is the defining equation for  $\mathcal{F}$ . So, the tangent space  $T(\mathcal{F}, F)$  is the subspace of (86) orthogonal to the gradient of the determinant. By Laplace expansion,

$$\frac{\partial \det(F)}{\partial f_{11}} = \det \begin{pmatrix} f_{22} & f_{23} \\ f_{32} & f_{33} \end{pmatrix},$$

$$\frac{\partial \det(F)}{\partial f_{12}} = -\det \begin{pmatrix} f_{21} & f_{23} \\ f_{31} & f_{33} \end{pmatrix},$$

$$\frac{\partial \det(F)}{\partial f_{13}} = \det \begin{pmatrix} f_{21} & f_{22} \\ f_{31} & f_{32} \end{pmatrix}.$$

$$D\Phi_1(w) = \left( \begin{array}{c|cccc} I_{15 \times 15} & & & & 0_{15 \times 5} \\ \hline \mathbf{R} & [e_1]_{\times} \mathbf{R} \Gamma_1 & [e_2]_{\times} \mathbf{R} \Gamma_1 & [e_3]_{\times} \mathbf{R} \Gamma_1 & \hat{\mathbf{T}}_1^{\perp} & \hat{\mathbf{T}}_2^{\perp} \\ & \ddots & & & \vdots & \vdots \\ & & \mathbf{R} & [e_1]_{\times} \mathbf{R} \Gamma_5 & [e_2]_{\times} \mathbf{R} \Gamma_5 & [e_3]_{\times} \mathbf{R} \Gamma_5 & \hat{\mathbf{T}}_1^{\perp} & \hat{\mathbf{T}}_2^{\perp} \end{array} \right)$$

Fig. 14. Jacobian matrix for the differential of (M-28) at  $w = (\mathbf{R}, \hat{\mathbf{T}}, \Gamma_1, \dots, \Gamma_5)$ . This is used to compute the condition number of the 5-point problem.

$$G = \begin{pmatrix} \hat{\mathbf{T}}_1^2 + 1 & \hat{\mathbf{T}}_1 \hat{\mathbf{T}}_2 & \hat{\mathbf{T}}_1 \hat{\mathbf{T}}_3 & \hat{\mathbf{T}}_3(\hat{\mathbf{T}}_1^{\perp})_2 - \hat{\mathbf{T}}_2(\hat{\mathbf{T}}_1^{\perp})_3 & \hat{\mathbf{T}}_3(\hat{\mathbf{T}}_2^{\perp})_2 - \hat{\mathbf{T}}_2(\hat{\mathbf{T}}_2^{\perp})_3 \\ \hat{\mathbf{T}}_1 \hat{\mathbf{T}}_2 & \hat{\mathbf{T}}_2^2 + 1 & \hat{\mathbf{T}}_2 \hat{\mathbf{T}}_3 & -\hat{\mathbf{T}}_3(\hat{\mathbf{T}}_1^{\perp})_1 + \hat{\mathbf{T}}_1(\hat{\mathbf{T}}_1^{\perp})_3 & -\hat{\mathbf{T}}_3(\hat{\mathbf{T}}_2^{\perp})_1 + \hat{\mathbf{T}}_1(\hat{\mathbf{T}}_2^{\perp})_3 \\ \hat{\mathbf{T}}_1 \hat{\mathbf{T}}_3 & \hat{\mathbf{T}}_2 \hat{\mathbf{T}}_3 & \hat{\mathbf{T}}_3^2 + 1 & \hat{\mathbf{T}}_2(\hat{\mathbf{T}}_1^{\perp})_1 - \hat{\mathbf{T}}_1(\hat{\mathbf{T}}_1^{\perp})_2 & \hat{\mathbf{T}}_2(\hat{\mathbf{T}}_2^{\perp})_1 - \hat{\mathbf{T}}_1(\hat{\mathbf{T}}_2^{\perp})_2 \\ \hat{\mathbf{T}}_3(\hat{\mathbf{T}}_1^{\perp})_2 - \hat{\mathbf{T}}_2(\hat{\mathbf{T}}_1^{\perp})_3 & -\hat{\mathbf{T}}_3(\hat{\mathbf{T}}_1^{\perp})_1 + \hat{\mathbf{T}}_1(\hat{\mathbf{T}}_1^{\perp})_3 & \hat{\mathbf{T}}_2(\hat{\mathbf{T}}_1^{\perp})_1 - \hat{\mathbf{T}}_1(\hat{\mathbf{T}}_1^{\perp})_2 & 2 & 0 \\ \hat{\mathbf{T}}_3(\hat{\mathbf{T}}_2^{\perp})_2 - \hat{\mathbf{T}}_2(\hat{\mathbf{T}}_2^{\perp})_3 & -\hat{\mathbf{T}}_3(\hat{\mathbf{T}}_2^{\perp})_1 + \hat{\mathbf{T}}_1(\hat{\mathbf{T}}_2^{\perp})_3 & \hat{\mathbf{T}}_2(\hat{\mathbf{T}}_2^{\perp})_1 - \hat{\mathbf{T}}_1(\hat{\mathbf{T}}_2^{\perp})_2 & 0 & 2 \end{pmatrix}$$

Fig. 15. Gram matrix for basis (88) of the tangent space to essential matrices. This is used to compute the condition number for the 5-point problem.

$$D\Phi_1(w) = \left( \begin{array}{c|ccc} I_{21 \times 21} & & & 0_{21 \times 7} \\ \hline \mathbf{M}(b)(:, 1 : 3) & \frac{\partial \mathbf{M}(b)}{\partial b_1} \begin{pmatrix} \Gamma_1 \\ 1 \end{pmatrix} & \dots & \frac{\partial \mathbf{M}(b)}{\partial b_7} \begin{pmatrix} \Gamma_1 \\ 1 \end{pmatrix} \\ & \vdots & & \vdots \\ & \mathbf{M}(b)(:, 1 : 3) & \frac{\partial \mathbf{M}(b)}{\partial b_1} \begin{pmatrix} \Gamma_7 \\ 1 \end{pmatrix} & \dots & \frac{\partial \mathbf{M}(b)}{\partial b_7} \begin{pmatrix} \Gamma_7 \\ 1 \end{pmatrix} \end{array} \right)$$

Fig. 16. Jacobian matrix for the differential of (M-32) at  $w = (b, \Gamma_1, \dots, \Gamma_7)$ . This is used to compute the condition number for the 7-point problem. Here  $\mathbf{M}(b)$  is like in Lemma M-4, regarded as in  $\mathbb{R}^{3 \times 4}$ , and  $\mathbf{M}(b)(:, 1 : 3)$  is the left  $3 \times 3$  submatrix. The relevant Gram matrix was given in (94).

By Cramer's rule, this vector spans the right kernel of

$$\begin{pmatrix} f_{21} & f_{22} & f_{23} \\ f_{31} & f_{32} & f_{33} \end{pmatrix} \quad (90)$$

if (90) has rank 2, or else it is 0. Thus the first row of  $\nabla \det(F)$  is proportional to  $\mathbf{e}$ . Similarly, the second and third rows of  $\nabla \det(F)$  are proportional to  $\mathbf{e}$ , because  $\mathbf{e}$  spans the right kernel of  $F$ . Likewise, each column of  $\nabla \det(F)$  is proportional to the left epipole  $\mathbf{e}'$  of  $F$ . Moreover,  $\nabla \det(F)$  does not vanish because  $F$  has rank 2. It follows that the gradient is a nonzero scalar multiple of  $\mathbf{e}'\mathbf{e}^{\top}$ . The lemma is clear.  $\square$

A particular non-orthonormal basis of the tangent space appears in our condition number formula. Namely, one can build fundamental matrices using the parameterization

$\mathbf{M}(b)$  in Lemma M-4 for world scenes and the formula after (M-13) for  $F$ . Doing so parameterizes  $\mathcal{F}$  as

$$F(b) = \begin{pmatrix} b_4 & b_5 & b_6 \\ -1 & -b_1 & -b_2 \\ -b_3 b_4 + b_7 & -b_3 b_5 + b_1 b_7 & -b_3 b_6 + b_2 b_7 \end{pmatrix}. \quad (91)$$

The relevant basis for  $T(\mathcal{F}, F)$  is then

$$DF(b)(e_1), \dots, DF(b)(e_7). \quad (92)$$

Note that  $DF$  may be computed as  $DF_3 \circ DF_2 \circ DF_1$ , where  $F_1 : \mathbb{R}^7 \rightarrow \mathbb{R}^{3 \times 3}$  is the same as (91) but with output regarded as in Euclidean space,  $F_2 : \mathbb{R}^{3 \times 3} \rightarrow \mathbb{S}^8$  sends  $M$  to  $M/\|M\|_F$ , and  $F_3 : \mathbb{S}^8 \rightarrow \mathbb{P}(\mathbb{R}^{3 \times 3})$  is the natural quotient

map. One checks that  $DF_1(b)$  is represented by

$$J = \begin{pmatrix} 0 & 0 & 0 & 1 & 0 & 0 & 0 \\ 0 & 0 & 0 & 0 & 1 & 0 & 0 \\ 0 & 0 & 0 & 0 & 0 & 1 & 0 \\ 0 & 0 & 0 & 0 & 0 & 0 & 0 \\ -1 & 0 & 0 & 0 & 0 & 0 & 0 \\ 0 & -1 & 0 & 0 & 0 & 0 & 0 \\ 0 & 0 & -b_4 & -b_3 & 0 & 0 & 1 \\ b_7 & 0 & -b_5 & 0 & -b_3 & 0 & b_1 \\ 0 & b_7 & -b_6 & 0 & 0 & -b_3 & b_2 \end{pmatrix}, \quad (93)$$

$DF_2(F_1(b))$  sends  $\dot{M} \mapsto \frac{1}{\|F_1(b)\|_F} \dot{M} - \frac{\langle \dot{M}, F_1(b) \rangle}{\|F_1(b)\|_F^3} F_1(b)$ , and  $DF_3$  is the identity up to the identification (86).

We can orthonormalize (92) using Lemma 28. The associated Gram matrix works out to:

$$G = \frac{1}{\|f\|_2^2} J^\top J - \frac{1}{\|f\|_2^4} (J^\top f)(J^\top f)^\top \in \mathbb{R}^{7 \times 7}, \quad (94)$$

with  $J$  as in (93) and  $f = \text{vec}(F_1(b))$ .

## APPENDIX M

### BACKGROUND ON PLÜCKER COORDINATES

In algebraic geometry, it is well-known that the set of codimension- $d$  linear subspaces of  $\mathbb{P}_{\mathbb{R}}^n$  is an irreducible smooth projective variety, called the **Grassmannian**:

$$\text{Gr}(\mathbb{P}_{\mathbb{R}}^{n-d}, \mathbb{P}_{\mathbb{R}}^n) = \{L \subseteq \mathbb{P}_{\mathbb{R}}^n : \dim(L) = n - d\}.$$

In Theorem M-13 and Section M-6.2, we use a classic coordinate system (more precisely, embedding) for the Grassmannian.

To explain it, let  $L \in \text{Gr}(\mathbb{P}_{\mathbb{R}}^{n-d}, \mathbb{P}_{\mathbb{R}}^n)$ . Write  $L$  as the kernel of a full-rank matrix  $M \in \mathbb{R}^{d \times (n+1)}$ . The **primal Plücker coordinates** of  $L$  are defined as the maximal minors of  $M$ :

$$p(L) = \left( p_{\mathcal{I}}(L) := \det(M(:, \mathcal{I})) : \mathcal{I} \in \binom{[n+1]}{d} \right)$$

It turns out this is a well-defined point in  $\mathbb{P}_{\mathbb{R}}^{\binom{n+1}{d}-1}$ , independent of the choice of  $M$ . Alternatively we can write  $L$  as the row span of a full-rank matrix  $N \in \mathbb{R}^{(n-d+1) \times (n+1)}$ . The **dual Plücker coordinates** of  $L$  are the maximal minors of  $N$ :

$$q(L) = \left( q_{\mathcal{J}}(L) := \det(N(:, \mathcal{J})) : \mathcal{J} \in \binom{[n+1]}{n+1-d} \right).$$

Again this is a well-defined point  $\mathbb{P}_{\mathbb{R}}^{\binom{n+1}{d}-1}$ , independent of the choice of  $N$ . Actually, the primal and dual coordinates are equal up to permutation and sign flips. Specifically,

$$\left( p_{\mathcal{I}}(L) : \mathcal{I} \in \binom{[n+1]}{d} \right) = \left( (-1)^{n+|\mathcal{I}|} q_{[n+1] \setminus \mathcal{I}}(L) : \mathcal{I} \in \binom{[n+1]}{d} \right)$$

where  $|\mathcal{I}| := \sum_{i \in \mathcal{I}} i$ .

In Theorem M-13, the polynomial  $\mathbf{P}_y$  is in  $\binom{n+1}{d}$  variables. The variables are the primal Plücker coordinates of the subspace  $\ker \mathbf{L}(x)$  in  $\mathbb{P}_{\mathbb{R}}^n$ , i.e. the maximal minors of  $\mathbf{L}(x)$ .